Effects of the terms associated with ϕ_{zz} in free surface condition on the attitudes and resistance of different ships

Yunbo Li[a,c], Jiaye Gong[a], Qingwei Ma*[,a,b], Shiqiang Yan[b]

[a] College of Shipping Building Engineering, Harbin Engineering University, China
[b] School of Mathematics, Computer Science and Engineering, City, University of London
[c] College of Ocean Science and Engineering, Shanghai Maritime University, China
*Corresponding Author: q.ma@city.ac.uk

Abstract:

One of approaches for numerical simulation of a ship moving in a still water is based on the composition of double-body flow and wavy flow solved by a boundary element method. There are several terms related to the second order derivative (ϕ_{zz}) of double-body flow velocity potential with respect to the vertical coordinate in the free surface conditions. Understanding of the effects of the terms is very limited so far. In many cases, they are just ignored even for ships with a high forward speed, particularly in the cases associated with multihull ships, for which no investigations on their effects have been found. This paper will present a study on the effects of the terms on the numerical prediction of the attitudes and resistance of different ships in various situations, including monohull, catamaran and trimaran with different parameters and at different Froude numbers. The results will demonstrate that the effects of the terms are significant in many cases and that considering this term may lead to the results similar to those obtained by fully nonlinear models at high Froude numbers.

Key Words: attitudes of ships, sinkage, trim, potential theory, monohull, catamaran, trimaran

1 Introduction

In the process of ship design, hull attitudes including trim and sinkage are very important parameters, because they may have significant effect on propeller design and hull form optimization. Ma et al. (2016) showed that the trim and sinkage were quite large when the Froude number reaches 0.45 based on experimental measurements for 22 monohull ship models. The influence of sinkage and trim on the drag of a ship can be significant for $\text{Froude Number} > 0.25$, depending on the hull form, as indicated by Ma et al. (2017). For high-speed ships, the hull attitude has even more significant effect on the resistance calculation, as pointed out by Deng et al. (2015), which took sinkage and trim into account for trimaran resistance calculation, and found the resistance of the main hull and side hull to be increased by 18% and 200%, respectively, at $\text{Froude Number} = 0.65$.

Several approaches have been developed for predicting the hull attitudes and their resistance. The CFD methods may be employed, but they are very computationally expensive and unsuitable for a large amount of computation in the early stage of ship design. Sherbaz (2014) demonstrated that pressure forces have a far greater effect on trimming moments compared with viscous forces. Therefore, the methods based on potential flow theory are often employed, which can give results with sufficient accuracy but is much faster. One of the potential flow methods was proposed by Raven (1994, 1996), called Rapid (Raised panel improved Dawson) method. In his method, the consideration of nonlinear effects was achieved by iteration. In each iteration, the high-order terms in the free surface conditions are omitted. Another nonlinear potential method is based on a panel method using Rankine source as a Green's function, as described by Wang et al. (2011). In their method, the nonlinear free surface conditions were satisfied also by performing iterations and the nonlinearity was fully considered in each iteration. Chen et al. (2016) used the similar iterative method but employed the fully nonlinear high order boundary element method and started with a solution obtained by using a linear method. They studied the hull attitudes of Wigley hull, KCS and a fishery patrol boat.

Another method based on the potential theory was proposed by Dawson (1977). In his method, the total flow is considered as the composition of double-body flow and wavy flow (also called perturbation flow in literature). The double-body flow is first solved satisfying the boundary conditions on the hull without the free surface. The wavy flow is then solved satisfying the conditions on both the hull surface and on the free surface. The free surface condition for the wavy flow is simplified on the basis of the double-body flow by assuming the Froude number to be small (i.e., the forward motion is slow). The advantage of Dawson's method is of its high computational efficiency compared with the other potential methods discussed above. Many researchers have improved this method. A few examples are just given here. Tarafdera et al. (2008a, 2008b) improved the Dawson's method with the body-fitted free surface mesh scheme instead of traditional streamline mesh scheme. The improved method was used to predict the wave-making resistance of ship with fixed trim and sinkage. Peng et al. (2014) improved the Dawson's method with a stern region excluded from the computational region to predict the wave making resistance of ships.

The Dawson's method including these with improvements has been employed by many researchers to analyze the attitudes and resistance of ships and to perform hull form optimization. Suzuki et al. (2005) carried out a stern hull form optimization for a ship with block coefficient $C_b > 0.65$ by using Dawson's method. Chen et al. (2006) using this method calculated the wave making resistance of high speed ($F_n > 0.7$) catamaran and trimaran with assuming that there were no trim and sinkage. Xie et al. (2007a, 2007b) also applied Dawson's method with more nonlinear terms to the analysis of 3D hydrofoil under free surface and wave-making resistance of a multi-hull craft for the Froude

number at 0.2 and 0.7 respectively. Yasin et al. (2008) also calculated 3D hydrofoil on and under free surface with a larger Froude number up to 0.8. Zhang et al. (2009, 2012) optimized S60 ships with bow bulbs based on the double-body flow theory and linearized free surface boundary condition. Xie et al. (2011) improved the hull form of a fishing trawler with Dawson's method and calculated the resistance in calm water. Skejic et al. (2012) used the improved Dawson's method to study the power performance and environmental footprint of high-speed ($F_n = 1.0$) vessels in calm deep water. Saha et al. (2013) computed the flow around the transom stern of a slim ship with the Froude number being up to 0.8. Ali et al. (2013) studied the bow wave breaking of a large block coefficient ship also using the Dawson's method. Lv et al. (2013) predicted the wave-making resistance of HUST hull ($C_b > 0.7$) form with different displacements and hull attitudes by using the method similar to Dawson's method. Mon et al. (2014) also applied the method to optimize a ship with a large block coefficient for reducing the wave-making resistance and wave breaking at the bow. Danışman (2014) optimized a fast catamaran with center bulb for the Froude number up to $F_n = 0.7$. Zhang et al. (2015a) applied the method to determine the hull form with minimum total resistance, and suggests that, compared with wave making resistance, there is no significant increase in viscous resistance during the process of hull form optimization. Zhang et al. (2015b) combined Dawson's method with vortex lattice method to optimize the full form ship ($C_b = 0.82$). Vernengo et al. (2017) used the same idea as of the Dawson's method, i.e., linearizing free surface condition around the double body flow to calculate the hydrodynamic resistance of small water plane area twin hulls (SWATHs) with the Froude number up to 0.9.

Although the Dawson's method has been extensively used by many researchers, not only for small Froude number (or low-speed on which the method is based) but also for large Froude numbers, the simplified free surface boundary conditions in Dawson (1977) was not based on a sound theoretical analysis as indicated by Eggers (1980) and Nakos (1990). To overcome the shortcoming, Eggers (1980) and Nakos (1990) gave two forms of free surface conditions by keeping the terms containing 4^{th} order of Froude number. Compared with the free surface boundary conditions in Dawson (1977), both Eggers (1980) and Nakos (1990) contained the additional terms associated with the second order derivative (ϕ_{zz}) of the double-body flow potential. There is a slight difference between the free surface conditions in Nakos (1990) and Eggers (1980). The former has an additional term related to the product of the free surface elevation due to the double-body flow and ϕ_{zz} but no such terms in the later. So far, very limited investigations on the effects of the terms associated with ϕ_{zz} have been carried out. Most of the papers that apply Dawson's method or its improved forms just ignored the terms. Baba (1979) partially studied such effects on a monohull and proved that the effects can be significant for non-wall-sided ships. Xie et al (2007a, 2007b, 2016) did include the term in their

calculation of wave making resistance, but they did not investigate the effect of ϕ_{zz}. So, it is still an open question about what a role would be played by the term, in particular when the Froud number is quite large.

This paper aims to study the effects of the terms associated with ϕ_{zz} on the hull attitudes and corresponding wave-making resistance. Different ships including monohull, catamaran and trimaran will be considered. The evidence will be presented that the term ϕ_{zz} should be considered to obtain more accurate results.

2 Mathematical formulation and numerical method

The mathematical formulation and numerical methods for the problem concerned have been well known. A brief discussion about them are just given for completeness in this section.

2.1 Basic equations

The co-ordinate system moves with the same forward speed as the ship with its origin on the undisturbed free surface at midship. The *x*-axis and *y*-axis extend to stem and portside, respectively (Fig. 1). Ship advances with a constant speed U along the *x*-direction. It is assumed that the fluid is ideal and water depth is infinite.

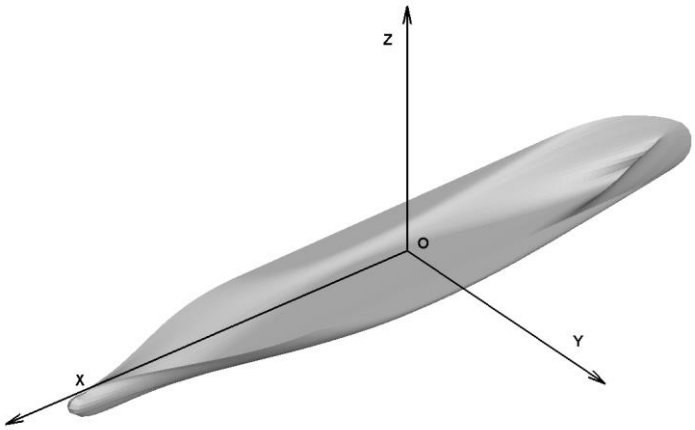

Fig. 1 Definition of the co-ordinate system

The total velocity potential ψ satisfies the Laplace equation

$$\nabla^2\psi = 0 \tag{1}$$

The total velocity potential ψ can be split into the double-body flow velocity potential ϕ and the wavy velocity potential φ representing the effect of the free surface conditions as suggested by Dawson (1977):

$$\psi = \phi + \varphi \tag{2}$$

$$\zeta = \xi + \eta \tag{3}$$

where ζ, ξ and η are the wave elevations corresponding to ψ, ϕ and φ, respectively. On the wetted hull surface, the normal velocity components of both the double-body flow velocity potential ϕ and the wavy potential φ are zero

$$\nabla\phi \cdot \boldsymbol{n} = 0 \tag{4}$$

$$\nabla\varphi \cdot \boldsymbol{n} = 0 \tag{5}$$

where $\boldsymbol{n}$ is the normal vector of the hull surface. On the free surface, the total velocity potential ψ satisfies both the kinematic and dynamic conditions

$$\psi_x\zeta_x + \psi_y\zeta_y - \psi_z = 0 \quad \text{on } z = \zeta \tag{6}$$

$$g\zeta + \tfrac{1}{2}(\nabla\psi \cdot \nabla\psi - U^2) = 0 \quad \text{on } z = \zeta \tag{7}$$

Eliminating ζ from Eq. (6) and Eq. (7) leads to

$$g\psi_z + \tfrac{1}{2}\nabla\psi \cdot \nabla(\nabla\psi \cdot \nabla\psi) = 0 \quad \text{on } z = \zeta \tag{8}$$

Based on the slow-speed linearization (Nakos,1990) with the higher order of Froude number ignored, substituting Eq. (2) into Eq. (8) and expanding the resulting equation into the Taylor series, one obtains the following expression of the free surface condition in terms of ϕ and φ

$$g\varphi_z + \nabla\phi \cdot \nabla(\nabla\phi \cdot \nabla\varphi) + \frac{1}{2}\nabla\varphi \cdot \nabla(\nabla\phi \cdot \nabla\phi) - \frac{\partial}{\partial z}\left[g\phi_z + \frac{1}{2}\nabla\phi \cdot \nabla(\nabla\phi \cdot \nabla\phi)\right]\frac{\nabla\phi \cdot \nabla\varphi}{g + \nabla\phi \cdot \nabla\phi_z}$$

$$= -g\phi_z - \frac{1}{2}\nabla\phi \cdot \nabla(\nabla\phi \cdot \nabla\phi) + \frac{\partial}{\partial z}\left[g\phi_z + \frac{1}{2}\nabla\phi \cdot \nabla(\nabla\phi \cdot \nabla\phi)\right]\frac{\nabla\phi \cdot \nabla\phi - U^2}{2g}$$

$$\text{on } z = 0 \tag{9}$$

Because the double-body flow velocity potential ϕ is symmetric to the undisturbed free surface (Tarafdera et al., 2008a), it satisfies

$$\phi_z = 0$$

$$\nabla\phi \cdot \nabla\phi_z = 0 \qquad \text{on } z = 0 \tag{10}$$

$$\frac{\partial}{\partial z}[\nabla\phi \cdot \nabla(\nabla\phi \cdot \nabla\phi)] = 0$$

Substituting Eq. (10) into Eq. (9), the free surface condition can be re-written as

$$\phi_x\left(\phi_x\varphi_x + \phi_y\varphi_y\right)_x + \phi_y\left(\phi_x\varphi_x + \phi_y\varphi_y\right)_y + \frac{1}{2}\varphi_x\left(\phi_x^2 + \phi_y^2\right)_x + \frac{1}{2}\varphi_y\left(\phi_x^2 + \phi_y^2\right)_y + g\varphi_z$$

$$-\phi_{zz}(\phi_x\varphi_x+\phi_y\varphi_y)=\frac{1}{2}\phi_{zz}(\phi_x^2+\phi_y^2-U^2)-\frac{1}{2}\phi_x(\phi_x^2+\phi_y^2)_x-\frac{1}{2}\phi_y(\phi_x^2+\phi_y^2)_y$$

on $z=0$ (11)

It is noted that when Eq. (11) is applied to the region after the transom stern of a ship, the velocity at the intersection curve between the free surface and the transom needs to be estimated by an approximate approach. This paper follows the approximation proposed by Saha et al. (2013), in which the velocity is evaluated by Bernoulli's equation with the assumption that the flow at the intersection curve is tangential to the hull surface. The readers are referred to the cited reference for more details.

It is also noted that Eq. (11) has two terms related to ϕ_{zz} (the second order derivative of the double-body velocity potential along the vertical direction): one is the last term on the left-hand side associated with the wavy and double-body flow potentials while the other is the first term on the right-hand side associated only with the double-body flow potential. The equation here is the same as that in Nakos (1990) but different from that in Raven (1996) as the first term on the right hand side excluded in the latter. In the original formulation of Dawson (1977), both terms were omitted, which has been usually followed in literature (e.g, Tarafdera et al., 2008a). Baba (1979) studied the effects of the first term on the right-hand side without the last term on the left and proved its effects to be significant for the non-wall-sided ships. Study on the effects of the two terms is very limited so far. The main contribution of this paper is to investigate the effects of both the terms and to quantitively demonstrate that they should not be ignored in many cases. For convenience of discussions, the two terms including ϕ_{zz} are denoted as SOZ hereafter.

In addition, as the computation domain must be truncated at a finite distance from the ships and artificial boundaries need to be inserted around the ships, the radiation condition need to be imposed on the artificial boundaries, which should be $\nabla\phi=-U\vec{e}_x$ and $\nabla\varphi=0$ in the area far from the ships. With applying the correct radiation conditions, there should be no wave at the upstream free surface and the downstream reflected wave will not significantly affect wave dynamics near the ships. Based on the discussions of Nakos (1990), the imposition of the upstream radiation conditions should be carefully dealt with while the downstream radiation condition does not affect the results considerably as long as the truncated boundaries are reasonably far away from the ships. Numerical implementation of the radiation condition will be discussed in the sections below.

2.2 Numerical method and procedure for solving the velocity potentials

Following the conventional boundary element method, e.g., (Dai, 2008), the double-body velocity potential (Fig. 2) ϕ can be expressed as

$$\phi = \iint_{S_B+S_B'} \frac{1}{r}\sigma_{B0}\, dS - Ux \tag{12}$$

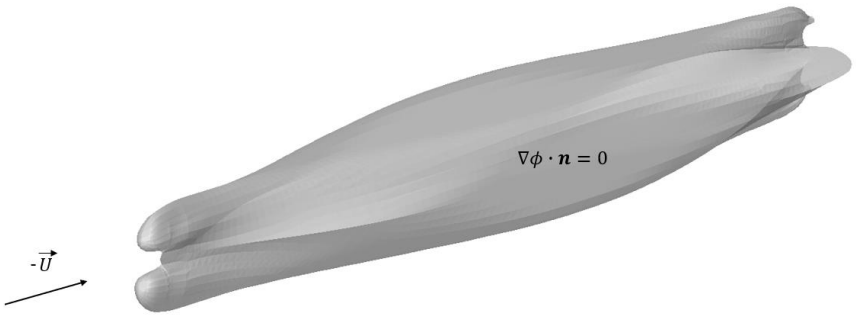

Fig. 2 Sketch of a double body model

where S_B is the hull surface boundary, and S_B' is the image of S_B about the undisturbed free surface $z = 0$, r is the distance from the source point to the field point. It is noted that the corresponding source σ_{B0} on S_B' is equal to σ_{B0} on S_B due to symmetry. The discretized form of the double-body velocity potential at the field point i with the constant distribution of source on a panel can be expressed as

$$\phi_i = \sum_{j=1}^{N_B} (\sigma_{B0})_j \iint_{S_j+S_j'} \frac{1}{r_{ij}} dS - Ux \tag{13}$$

where r_{ij} represents the distance between the i-th and j-th points; S_j and S_j' are the panels on the hull surface and its image, respectively; N_B is the number of panels on the hull surface. The panels on the hull surface are triangular to conform to the curved hull surface as close as possible. Later, the free surface will also be discretized, which will be done by using quadrilateral panels. The reason why the panels on the free surface are quadrilateral, rather than triangular, is because the second order derivatives in Eq. (11) need to be estimated by using finite difference. Use of quadrilateral panels on the free surface makes the estimation of the second order derivatives relatively straightforward.

Using the hull surface condition Eq. (4), one obtains

$$-2\pi(\sigma_{B0})_i + \sum_{\substack{j=1 \\ i\neq j}}^{N_B} (\sigma_{B0})_j \iint_{S_j+S_j'} \nabla \frac{1}{r_{ij}} dS = \boldsymbol{U} \cdot \boldsymbol{n}_i \tag{14}$$

where the collocation point i is at the center of i-th panel, $\boldsymbol{n}_i$ is the normal vector in i-th panel of the hull surface, and $i = 1,2,\ldots,N_B$. The double-body velocity potential ϕ can be found after solving Eq. (14).

The integral in Eq. (14) represents the induced velocity at the field point i by an unit source on the panel S_j, which may be expressed as

$$V_{ij} = \left(v_{xij}, v_{yij}, v_{zij}\right) = \iint_{S_j} \nabla \frac{1}{r_{ij}} dS \tag{15}$$

Following the Hess-Smith approach (Dai, 2008; Raven, 1989), Eq. (15) is estimated in the local coordinate system (Fig. 3) of the panel S_j. The center of local coordinate system are the geometric center of the panel S_j. Take v_{zij} as example, the integration can be expressed as

$$v_{zij} = \sum_{k=1}^{N}\left(arctan\frac{m_{k,k+1}c_k - h_k}{z'_i r_k} - arctan\frac{m_{k,k+1}c_{k+1} - h_{k+1}}{z'_i r_{k+1}}\right) \tag{16}$$

$$c_k = (x'_k - x'_i)^2 + z'^2_i \qquad h_k = (x'_k - x'_i)(y'_k - y'_i) \tag{17}$$

$$m_{k,k+1} = \frac{y'_{k+1} - y'_k}{x'_{k+1} - x'_k} \qquad r_k = \sqrt{c_k + (y'_k - y'_i)^2} \tag{18}$$

where (x'_i, y'_i, z'_i) is the position of field point, (x'_j, y'_j, z'_j) is the position of source point, and (x'_k, y'_k, z'_k) is the k-th corner point of the panel j. $N = 3$ for a triangular panel on the hull surface, and $N = 4$ for a four-nodes panel on the free surface.

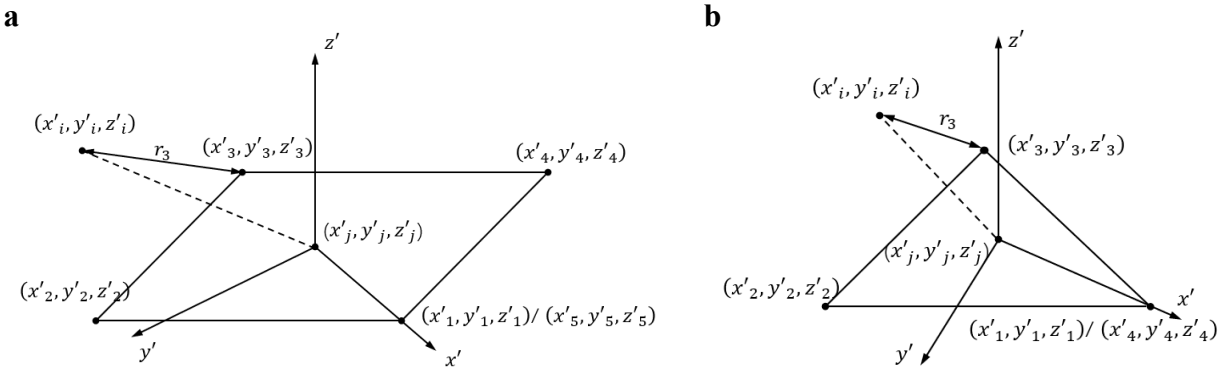

Fig. 3 Sketch of the local coordinate system. (a) a four-nodes panel on free surface, (b) a triangular panel on hull surface.

In the local coordinate system (x', y', z'), the normal vector is assumed to point to the inside hull on the hull surface panel and upward on the free surface panel. When $i = j$, the integration in Eq. (15) is analytically evaluated, i.e., $v_{zij} = 2\pi$. More details about the treatment could be found in Dai, (2008).

Using the solution of Eq. (14), the induced velocity ϕ_x and ϕ_y (ϕ_z) on the n-th field point of the free surface can be estimated by

$$(\phi_x)_n = \sum_{j=1}^{N_B}(\sigma_{B0})_j \iint_{S_j + S'_j} \frac{\partial}{\partial x}\left(\frac{1}{r_{nj}}\right) dS - U \tag{19}$$

$$(\phi_y)_n = \sum_{j=1}^{N_B}(\sigma_{B0})_j \iint_{S_j + S'_j} \frac{\partial}{\partial y}\left(\frac{1}{r_{nj}}\right) dS \tag{20}$$

ϕ_z can be found in the same way in Eq. (20), by changing y to z.

Similarly, the wavy velocity potential φ (Fig. 4) can be expressed by

$$\varphi = \iint_{S_B} \frac{1}{r}\sigma_{B1} dS + \iint_{S_f} \frac{1}{r}\sigma_f dS \tag{21}$$

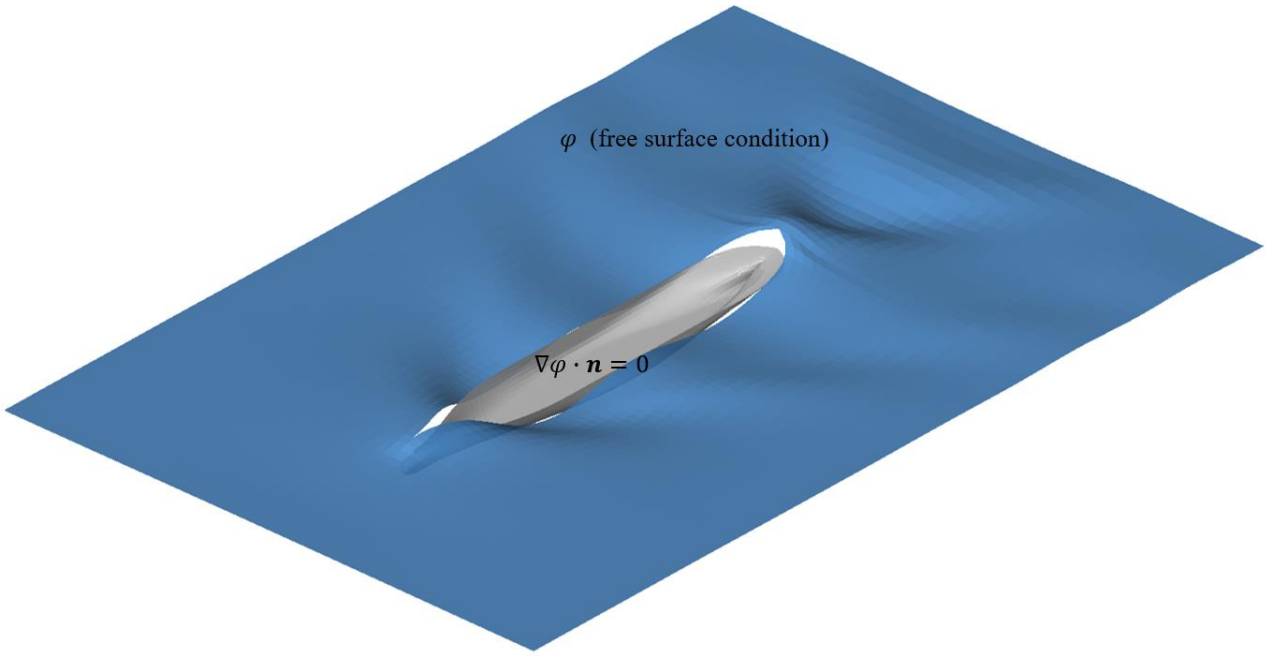

Fig. 4 Sketch of wavy velocity potential

where σ_{B1} and σ_f are the sources on the hull and free surface, respectively. Using the hull surface condition Eq. (5), one obtains

$$\sum_{\substack{j=1 \\ i\neq j}}^{N_B}(\sigma_{B1})_j \iint_{S_j} \frac{\partial}{\partial n_i}\left(\frac{1}{r_{ij}}\right) dS - 2\pi(\sigma_{B1})_i + \sum_{m=1}^{N_f}\left(\sigma_f\right)_m \iint_{S_m} \frac{\partial}{\partial n_i}\left(\frac{1}{r_{im}}\right) dS = 0 \tag{22}$$

where N_f is the number of the free surface panels.

The major difference between solving ϕ and φ is that the latter has to satisfy Eq. (11), the free surface condition. In other words, Eq. (22) should be solved together with Eq. (11). To discretize Eq. (11), one needs to evaluate the second order partial derivatives of products of velocity potential on the free surface panels. Take the $(\phi_x\varphi_x)_n$ on n-th free surface panel as example which can be expressed by

$$f_n = (\phi_x\varphi_x)_n = \sum_{j=1}^{N_B}(\phi_x)_n(I_x)_{nj}(\sigma_{B1})_j + \sum_{m=1}^{N_f}(\phi_x)_n(I_x)_{nm}\left(\sigma_f\right)_m$$

$$= \sum_{j=1}^{N_B} f(n,j) + \sum_{m=1}^{N_f} f(n,m), \tag{23}$$

$$(I_x)_{nj} = \iint_{S_j} \frac{\partial}{\partial x}\left(\frac{1}{r_{nj}}\right) dS, \qquad (I_x)_{nm} = \iint_{S_m} \frac{\partial}{\partial x}\left(\frac{1}{r_{nm}}\right) dS,$$

$$f(n,j) = (\phi_x)_n(I_x)_{nj}(\sigma_{B1})_j, \; f(n,m) = (\phi_x)_n(I_x)_{nm}\left(\sigma_f\right)_m.$$

The second order partial derivatives of the velocity potential can be found by estimating the first

order derivatives of f_n. Considering $\frac{\partial}{\partial x}f_n$ as an instance, one may have

$$\frac{\partial}{\partial x}f_n = \sum_{j=1}^{N_B}\frac{\partial}{\partial x}f(n,j) + \sum_{m=1}^{N_f}\frac{\partial}{\partial x}f(n,m) \tag{24}$$

Take $f(n,j)$ as instance, the partial derivative can be calculated as follows

$$\frac{\partial}{\partial x}f(n,j) = \frac{\partial}{\partial \xi}f(n,j)\frac{\partial \xi}{\partial x} + \frac{\partial}{\partial \eta}f(n,j)\frac{\partial \eta}{\partial x} \tag{25}$$

$$\frac{\partial}{\partial \xi}f(n,j) = [3f(n,j) - 4f(n-1,j) + f(n-2,j)]/2\Delta\xi \tag{26}$$

$$\frac{\partial x}{\partial \xi} = [3x(n) - 4x(n-1) + x(n-2)]/2\Delta\xi \tag{27}$$

$$\frac{\partial \xi}{\partial x} = \frac{1}{|J|}\frac{\partial y}{\partial \eta}, \quad \frac{\partial \eta}{\partial x} = -\frac{1}{|J|}\frac{\partial y}{\partial \xi}, \quad J = \begin{bmatrix} \partial x/\partial \xi & \partial x/\partial \eta \\ \partial y/\partial \xi & \partial y/\partial \eta \end{bmatrix} \tag{28}$$

where ξ and η are the vector components parallel to the local grid line, as shown in Fig. 5. More details about the finite difference scheme could be found in Tarafdera et al. (2008a,b). To satisfy the radiation conditions mentioned above, $\nabla\phi = -U\vec{e}_x$ and $\nabla\varphi = 0$ are applied on the foremost panel of the free surface when computing the second order partial derivatives as in shown in Eqs. (25)-(28).

Eqs. (25)-(28) works well for many cases. However, some spikes in the wave profiles near the bow and stern can be observed when Froude number is larger than 0.45. By numerical tests, it is found that the problem can be overcome by using a low order (two-point) finite difference operator, i.e., $\frac{\partial}{\partial \xi}f(n,j) = [f(n,j) - f(n-2,j)]/\Delta\xi$ and $\frac{\partial x}{\partial \xi} = [x(n) - x(n-2))]/\Delta\xi$ rather than their counterparts in Eqs. (25)-(28) on the panels near the bow and stern is employed. The idea is borrowed from Tarafdera et al (2007), in which a three-point finite difference operator was used for Fn<0.35 and two-point finite difference operator was used for Fn>0.35 in the whole domain. However it is noted that the numerical method adopted by Tarafdera et al (2007) is a perturbation method which is different from the one employed in this paper. The tests on using the two-point finite difference operator in the whole domain are also carried out for the work in this paper but the results show that the accuracy can be significantly downgraded, though the spikes do not appear. Use of the two-point finite difference operator only on a few panels near the bow and stern can ensure the accuracy is relatively higher without the spikes. More investigations are needed in future to find the reason why the two-point finite difference operator can help removing spikes.

.

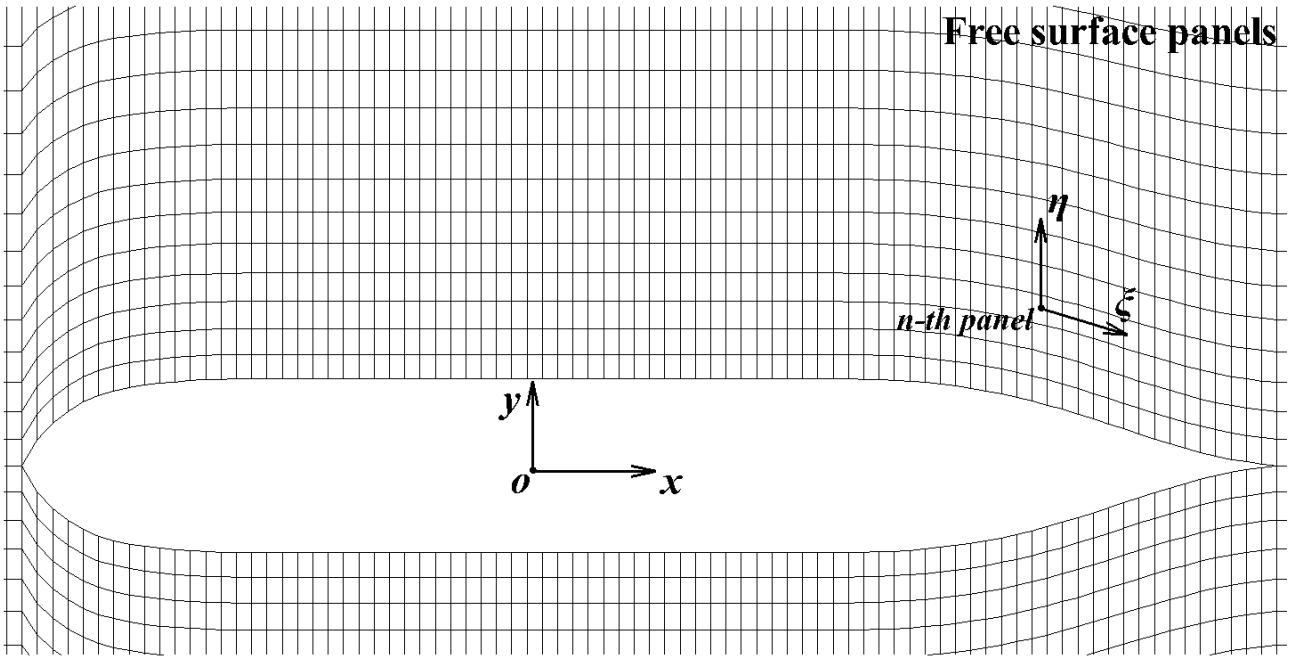

Fig. 5 Sketch of local coordinate system of free surface panel n

The term of ϕ_{zz} in the free surface condition is estimated in the following way

$$\phi_{zz}(x,y,0) = \frac{3\phi_z(x,y,0) - 4\phi_z(x,y,\Delta z) + \phi_z(x,y,2\Delta z)}{2\Delta z} \tag{29}$$

where Δz is proportional to the free surface panel length along x-direction, which is denoted by δL_p. Through convergent tests, Δz is taken as $0.05\delta L_p$. By solving Eq. (22) together with the discretized form of Eq. (11), the wavy velocity potential φ can be found.

To validate the method for computing ϕ_{zz}, Eq. (29) is applied to estimate the second order partial derivative of $\phi = \frac{1}{r}$, for which there should be $\phi_{zz} = \frac{4z^2}{r^5} + \frac{2}{r^3}$. In order to verify Eq. (29), the second order partial derivative at 10 points on the line from (0 0 0) to (0 1 0) with $\Delta z = -0.001$ are estimated by using Eq. (29) and compared with analytical values in Table 1. It can be seen that both results are in good agreement.

Table 1 Comparison between numerical result and analytical value of ϕ_{zz}.

No.	Field point			Analytical Value $\frac{4z^2}{r^5} + \frac{2}{r^3}$	Calculated by Eq. (29)
	x	y	z		
1	0	0.1	0	2000.000	2000.599
2	0	0.2	0	250.000	250.019
3	0	0.3	0	74.074	74.077
4	0	0.4	0	31.250	31.251
5	0	0.5	0	16.000	16.000
6	0	0.6	0	9.259	9.259
7	0	0.7	0	5.831	5.831
8	0	0.8	0	3.906	3.906

9	0	0.9	0	2.743	2.743
10	0	1.0	0	2.000	2.000

After finding the velocity potential and the velocity, the corresponding wave elevation at the n-th point of the free surface can be estimated by

$$\zeta_n = \frac{1}{2g}(|\boldsymbol{U}|^2 - |\boldsymbol{V}_n|^2) \tag{30}$$

where $\boldsymbol{V}_n = \nabla\phi_n + \nabla\varphi_n$.

Although the problem is steady relative to the coordinate system used, the attitudes (trim and sinkage) of the ships are unknown. To find the attitudes, the fact needs to be used that the ship will be in equilibrium and the resulting force coefficient C_{Fz} in the vertical direction and the moment coefficient C_{Ny} about the y-axis must be zero, i.e.,

$$C_{Fz} = \frac{\sum_{i=1}^{N_B} C_{pi} n_{zi} S_{wi} - \frac{2g\nabla_H}{U^2}}{\sum_{i=1}^{N_B} S_{wi}} = 0 \tag{31}$$

$$C_{Ny} = \frac{\sum_{i=1}^{N_B} C_{pi}[(z_i - z_g)n_{xi} - (x_i - x_g)n_{zi}]S_{wi}}{\sum_{i=1}^{N_B} x_i S_{wi}} = 0 \tag{32}$$

where the pressure coefficient on the hull surface is defined by $C_{pi} = 1 - \left(\frac{|\nabla\psi|}{U}\right)^2 + \frac{2gz_i}{U^2}$, S_{wi} is the area of i-th panel on the hull surface，x_i and z_i are the co-ordinates of the center of S_{wi}，x_g and z_g are the co-ordinates of ship gravitational center，n_{xi} and n_{zi} are the normal vector of S_{wi}, and ∇_H is the displacement of ship. It can be seen from the two equations above that C_{Fz} and C_{Ny} are related to the solutions of ϕ and φ, the solutions of ϕ and φ depend on the wetted surface of ships, which is related to their attitudes. As a result, Eqs. (33) and (34) can only be met through an iterative procedure as below:

(1) Given the values of sinkage (*S*) and trim (*T*) and the values of force and moment coefficients ($C_{Fz}{}^{(t)}$ and $C_{Ny}{}^{(t)}$) at *t*-th iteration (which are zero in the first iteration);

(2) Predict the values of sinkage (*S*) and trim (*T*) at (*t*+1)-th iteration by $S_{t+1} = S_t + C_{Fz}{}^{(t)}\delta_1$ and $T_{t+1} = T_t + C_{Ny}{}^{(t)}\delta_2$ with $\delta_1 = 0.0981\frac{F_n^2 L}{C_b B}$ and $\delta_2 = 0.0981\frac{F_n^2 L^2}{C_b B^2}$;

(3) Adjust grids on the wetted hull surface and on the free surface, and then find the solutions of ϕ and φ;

(4) Evaluate $C_{Fz}{}^{(t+1)}$ and $C_{Ny}{}^{(t+1)}$;

(5) Check if $\left|C_{Fz}{}^{(t+1)}\right| < \varepsilon$、$\left|C_{Ny}{}^{(t+1)}\right| < \varepsilon$ are satisfied; if yes, stop; otherwise go back to

Step (1).

The whole procedure is illustrated by the flow chart in Fig. 6. It has been numerically checked that $\varepsilon = 10^{-4}$ is appropriate and used in the paper. In the above procedure, the Froude number F_n is defined by $F_n = U/\sqrt{Lg}$, and the block coefficient C_b by $C_b = \nabla_H/(LBD)$, where g is the gravitational acceleration, L and B are the length and breadth of the waterline under the hydrostatic balance with D being the draft from the keel to the waterline. When all the iteration is completed, the coefficient of wave making resistance can be calculated as $C_w = (\sum_{i=1}^{N_B} C_{pi} n_{xi} S_{wi})/(\sum_{i=1}^{N_B} S_{wi})$.

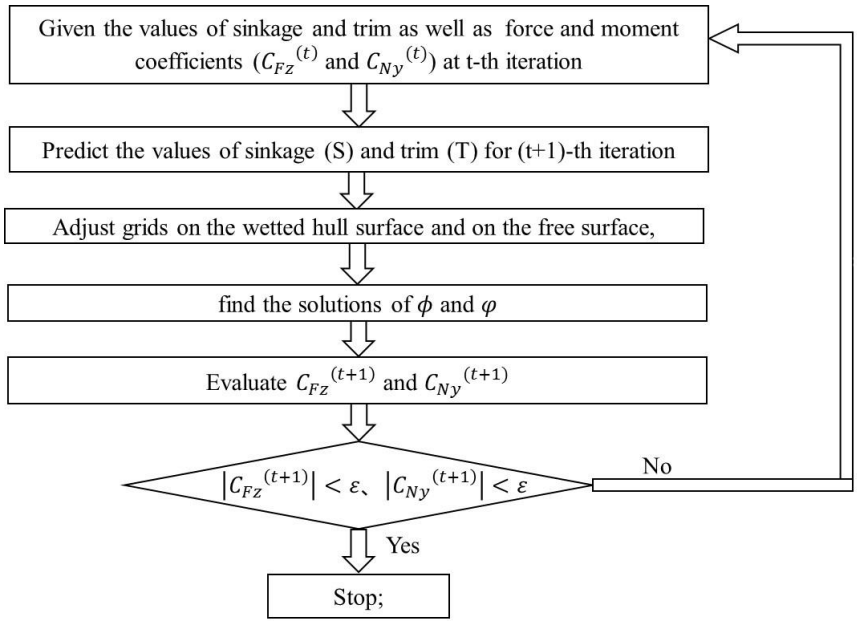

Fig. 6. Flow chart

3 Results and discussions

The effects of the SOZ terms will be investigated for different types of ships under different conditions, including monohull, trimaran and catamaran. In all the cases, the convergent tests will be carried out first to ensure that the elements used are small enough. In some cases, the numerical results are validated by experimental data.

3.1 Monohull

Wigley hull (IHI et al., 1983) and KRISO Container Ship (KCS) (Larsson et al., 2010) are taken as examples to study the effects of SOZ on the attitudes of monohull ships. The Wigley hull is considered first with its surface defined by

$$y = \frac{B}{2}\left[1 - (\frac{2x}{L})^2\right]\left[1 - (\frac{z}{D})^2\right] \tag{33}$$

The main characteristic dimensions of the Wigley hull are $B/L = 0.1$, $D/L = 0.063$, and its block

coefficient is $C_b = 0.444$, the gravity center is at $x_g/L = 0.0$ and $z_g/L = 0.0$.

The computational domain for the monohull cases are illustrated in Fig.7. The total length of the domain is $L_d = \alpha L + L + 1.5\alpha L$, where L is the waterline length of ship, αL is the length before the foremost point of the waterplane and $1.5\alpha L$ is the length after the aftmost point of the waterplane. The half width of the domain is $W_d = \alpha L$. Following the suggestion given by (Tarafdera et al., 2008a,b), $\alpha = 1.0$ is appropriate, which will be confirmed by some numerical results given below.

For the numerical computation, the meshes for the ship hull surface and the free surface are generated separately. The hull surface is firstly divided by a number of transversal and horizontal planes to give quadrilaterals, and then each of quadrilaterals are split into two triangles, to form the mesh as shown in Fig. 8. Refinement in the bow and stern areas is applied if necessary.

For generating the mesh for the free surface, it is split into three regions, shown in Fig. 7, by two lateral dashed lines. Region 1 covers the part of the free surface before the ship, Region 2 covers the part of the free surface between the foremost and aftmost points of waterplane and Region 3 covers the part of the free surface after the ship. When discretizing the free surface, Region 2 are firstly split by lateral lines, between which the distance is a constant determined by $2\pi LF_n^2/N_w$ with N_w being the number of panels per wavelength, as recommended by (Wang et al., 2011). Then, Regions 1 and 3 are split by lateral lines with variable distances, i.e., the distance expanded by the factor of 1.04 from dashed lines shown in Fig. 7. After that, the longitudinal lines are applied. The distance between the hull surface and its nearest longitudinal line is βL, while the distance between other longitudinal lines from the nearest longitudinal line expanded by factor of 1.04. The mesh generated in such way is illustrated in Fig. 9.

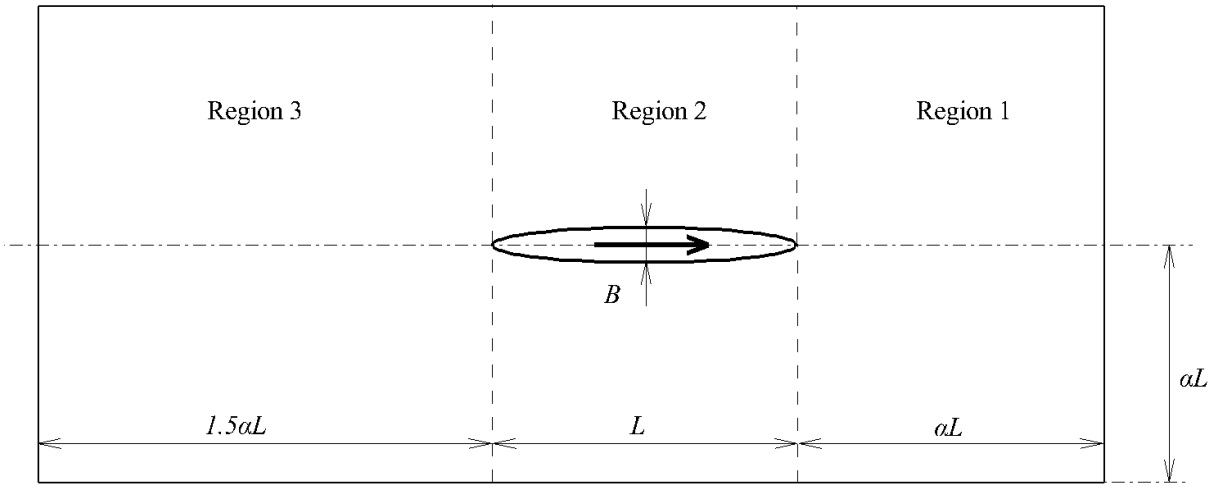

Fig. 7. Plan view of computation domain for monohull

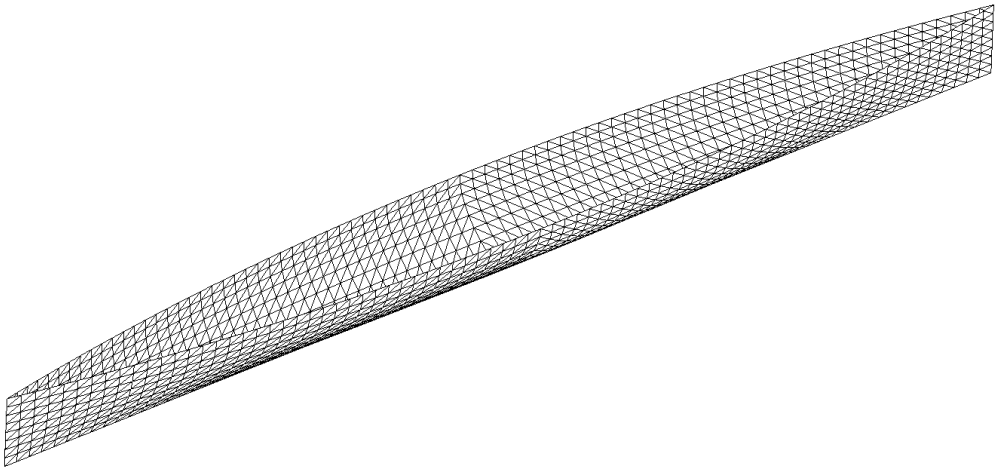

Fig. 8. Hull surface panel arrangement of the Wigley hull.

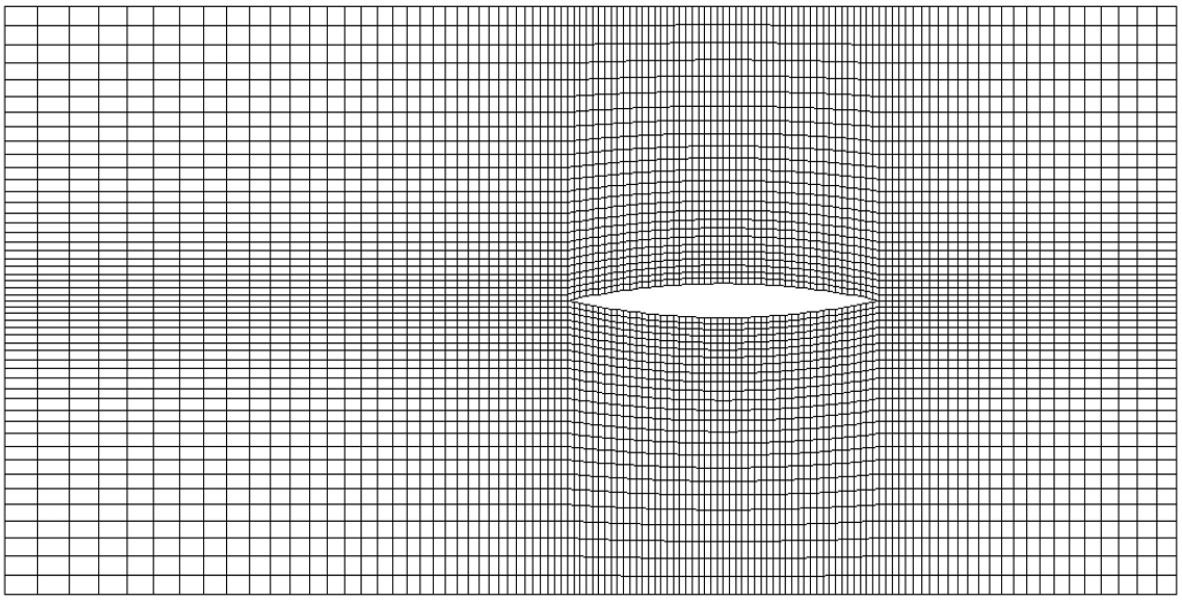

Fig. 9. Free surface panel arrangement of the Wigley hull (where NL and NT show the number of elements in transversal and longitudinal directions, respectively).

For the case with Froude number $F_n = 0.5$, the convergent tests for nine cases (each with different values of N_w and β) are carried out on a computer with Intel(R) Core(TM) i7-6700HQ CPU. The results for trim angle and sinkage together with the total CPU time are given in Table 2, in which the total CUP time is the time from first iteration step to the stable state with the trim and sinkage unchanged anymore. The relative errors are plot in Fig. 10, which is calculated by $|R_{i+1} - R_i|/|R_{i+1}|$, where R_i is the solution of either trim or sinkage for Case No. i.

Table 2

Computed result and the CPU time of Wigley hull with different panel arrangements at $F_n = 0.5$.

Case No.	Total grid number (on half domain)	Hull surface (half)	Free surface (half)	With SOZ		Without SOZ		Total CPU time
				Trim	Sinkage/L	Trim	Sinkage/L	
				deg	$*10^2$	deg	$*10^2$	min
1	1110	180	930	-2.034	-0.814	-2.094	-0.812	0.59
2	1544	320	1224	-1.936	-0.733	-1.987	-0.732	1.13
3	2077	500	1577	-1.897	-0.699	-1.948	-0.698	1.83
4	2673	720	1953	-1.880	-0.680	-1.928	-0.679	2.87
5	3349	980	2369	-1.867	-0.667	-1.915	-0.666	4.22
6	4030	1280	2750	-1.863	-0.654	-1.901	-0.657	7.38
7	4806	1620	3186	-1.853	-0.650	-1.899	-0.653	11.07
8	5625	2000	3628	-1.852	-0.651	-1.897	-0.650	16.87
9	7300	2880	4204	-1.854	-0.649	-1.898	-0.648	26.91

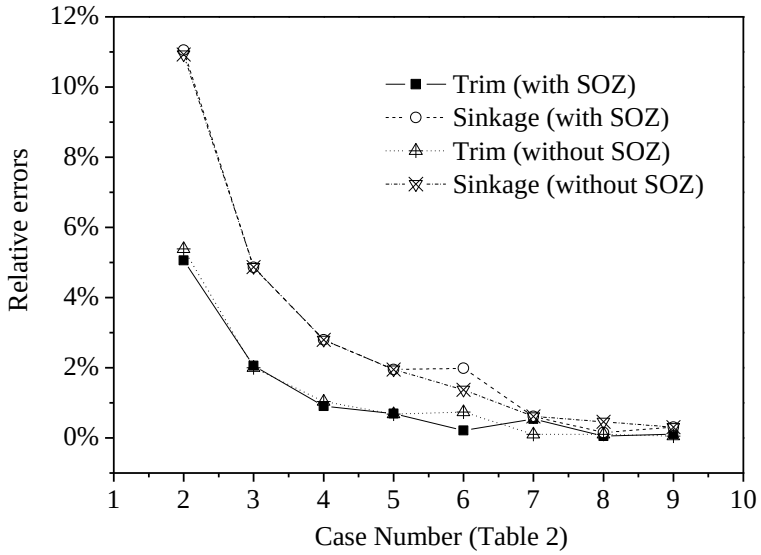

Fig. 10. Relative errors in solutions with and without SOZ (Wigley hull, $F_n = 0.5$).

Table 2 and Fig. 10 show that no matter whether the SOZ terms are included or not, the numerical results can be considered as convergent when the mesh is finer than that for No. 6 because the error are less than 2% in Cases 7, 8 and 9. To further demonstrate this, the wave profiles on the hull surface for Case 1, 3, 7 and 8 are depicted in Fig. 11, in which the maximum error between Case 7 and 8 occurring near the bow is 2.6%. Similar convergent tests are also carried out for the cases with smaller Froude number and confirmed that the meshes used in Case 7 are fine enough to achieve the convergent results, which is not presented for brief.

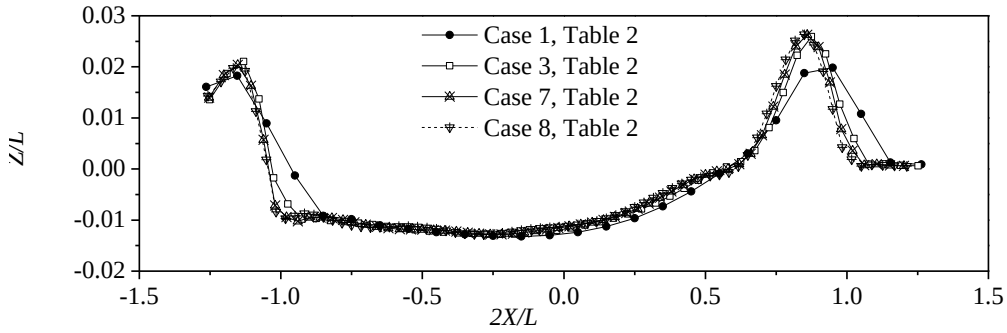

Fig. 11. Convergence of wave profiles with SOZ considered (Wigley hull, $F_n = 0.5$).

The free surface wave elevation of Case 8 is shown in Fig. 12, it can be seen that the wave before the ship is negligible and there is almost no visible disturbance due to the wave reflection on the lateral boundaries. This seems to mean that the numerical technique employed for the radiation condition is quite effective. To further show the effectiveness of the numerical technique for the radiation condition, the different values of α (different size of domain) are used for Case 7, and wave profiles at different longitudinal sections are shown in Fig. 13. It shows that there is no visible difference between the results for α=1 and α=2. The results with other values of α are also examined but not presented here as they indicate the same conclusion as these Fig. 13, i.e., the domain with α=1 is large enough and the influence of the reflected waves from the boundaries can be ignored.

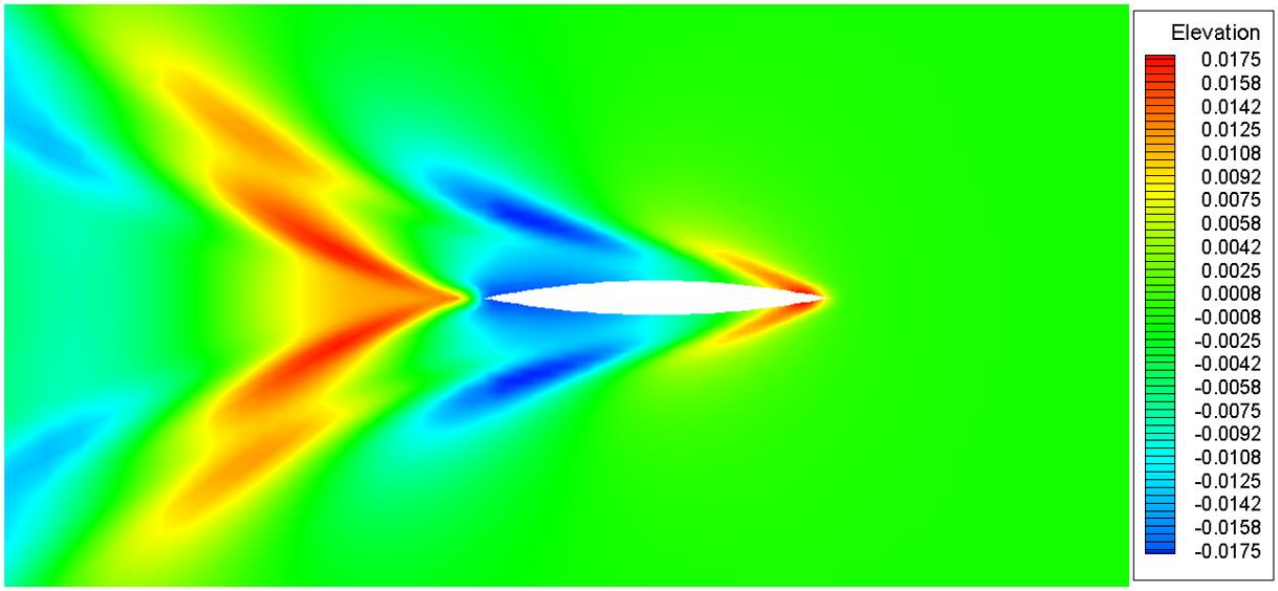

Fig. 12. Computed wave elevation of Wigley in Case 8 with SOZ terms at $F_n = 0.5$.

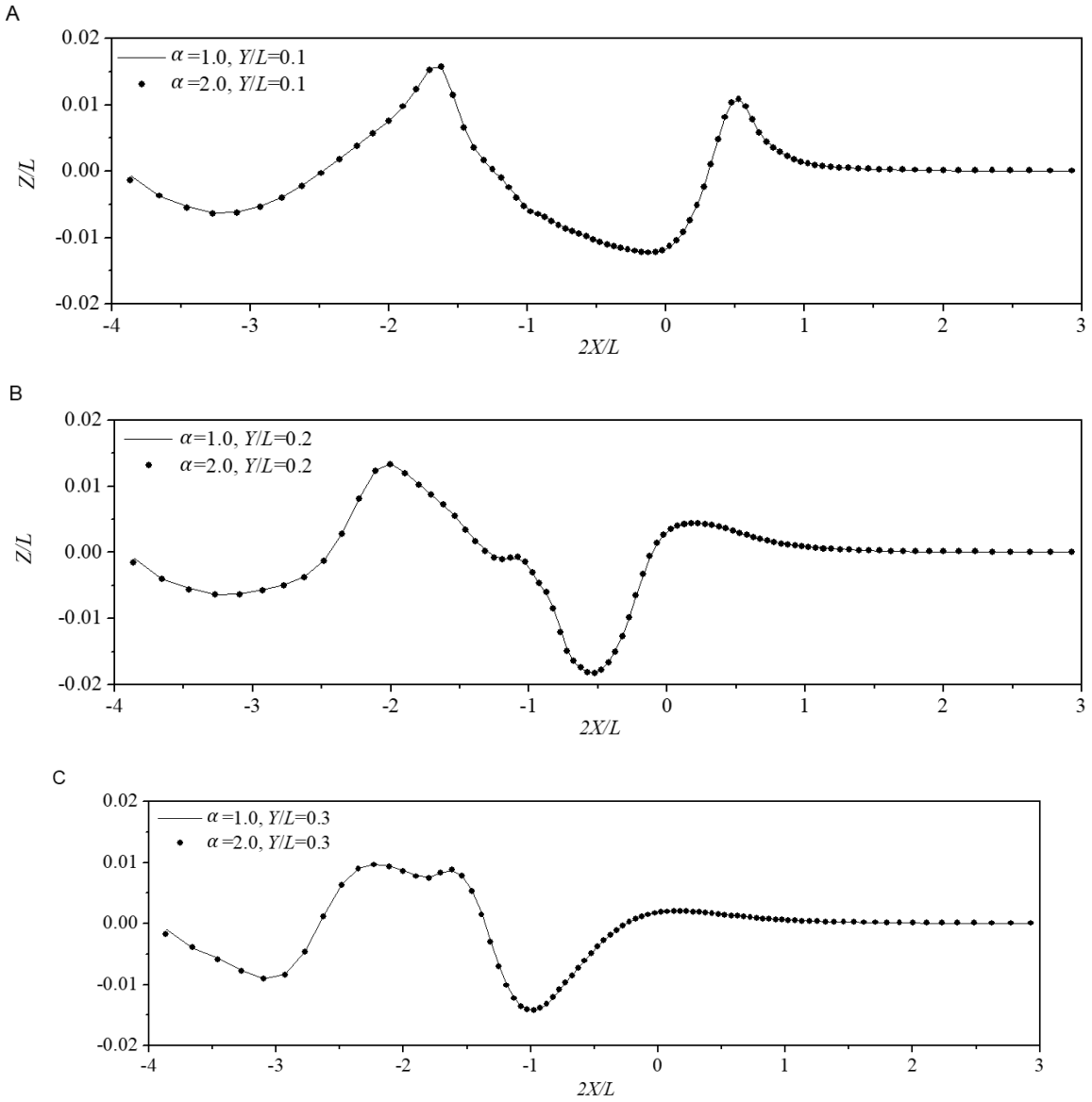

Fig. 13. Computed wave profiles of Wigley with SOZ terms at $F_n = 0.5$.

Based on the convergent study, the effects of the SOZ term on the sinkage and trim of the Wigley hull are studied for practical Froude number of a monohull. For this purpose, half the hull surface and free surface are discretized by 1620 panels and 3186 respectively, i.e. the same as in Case 7. Fig. 14. shows the computed results together with experimental data in literature (IHI et al., 1983). As can be seen, the SOZ terms have little effect on the numerical results for a range of Froude numbers less than 0.3. Only when Froude number is larger than 0.3, the terms begin to have visible effects on trim, and the results with the SOZ terms are a bit closer to the experimental data. However, the effect is not significant. To compare the numerical wave profiles with the experimental data (IHI et al., 1983) for the cases without trim and sinkage, the cases for the same ship at two Froude numbers are computed. The wave profiles on the hull are plotted in Fig. 15. The figure also shows that the effect of the SOZ terms on the wave profile is not significant and the wave profile with the SOZ term is

closer to experimental data.

a

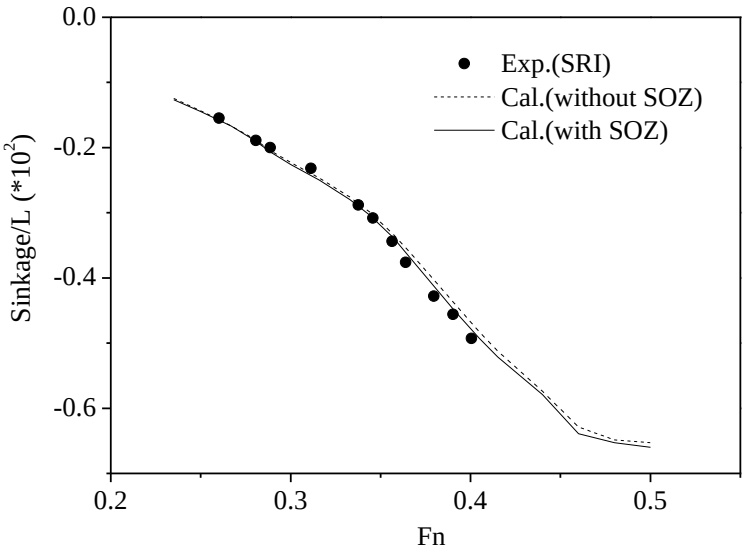

b

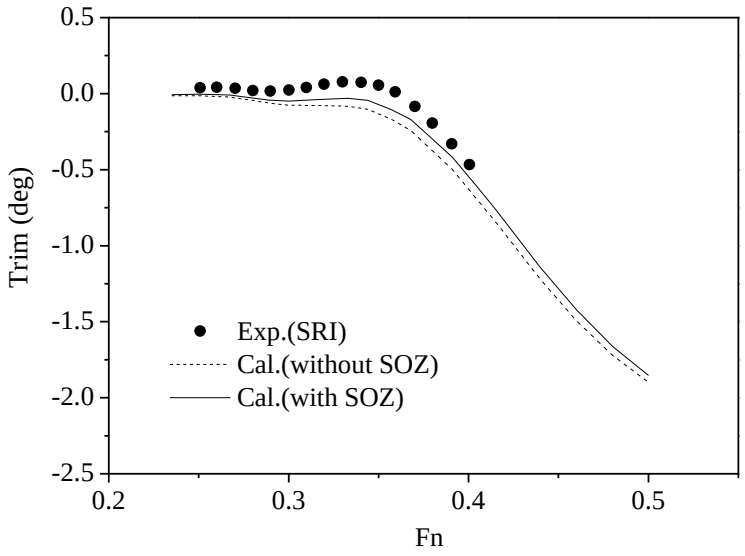

c

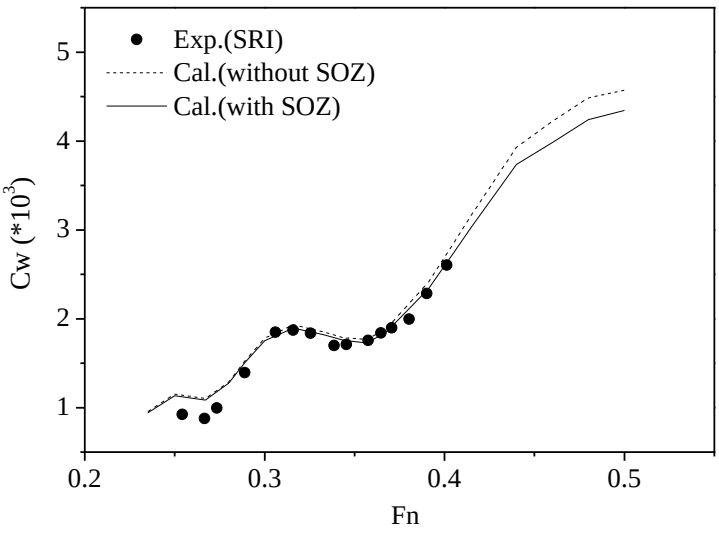

Fig. 14. Hull attitudes and wave-making resistance of Wigley hull. (a) Computed sinkage, (b) Computed trim. (c) wave making resistance

a

b

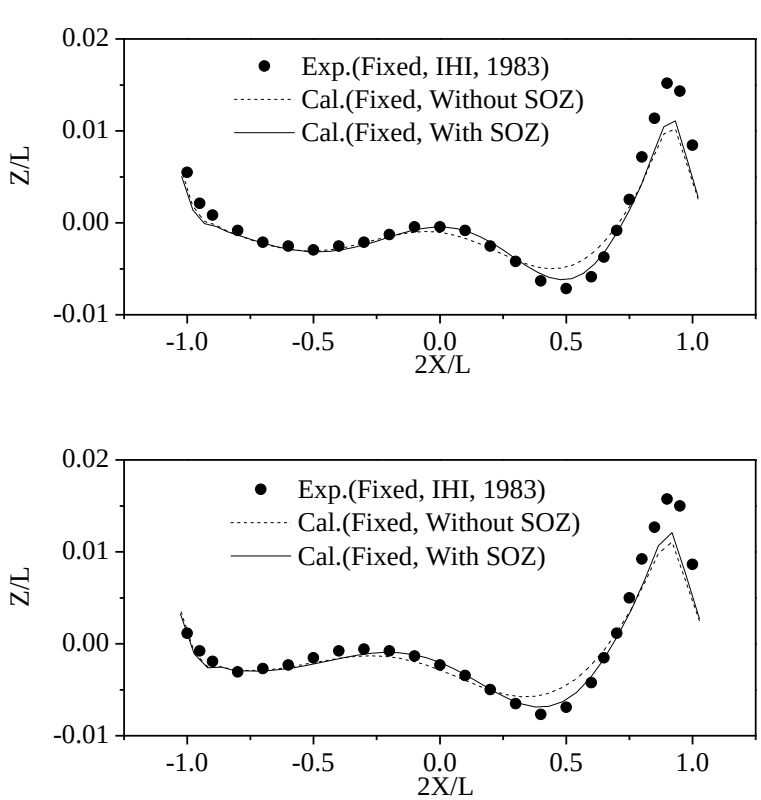

Fig. 15. Wave profiles of Wigley hull for different Froude numbers without trim and sinkage. (a) wave profiles at $F_n = 0.289$, (b) wave profiles at $F_n = 0.316$

Secondly, the effects of SOZ on the numerical results of KCS are studied. The main characteristic dimensions of KCS are $C_b = 0.65$, $D/L = 0.046$, $B/L = 0.139$, $x_g/L = -0.0149$, $z_g/L =$

-0.0149. The C_b and B/L are larger than those of the Wigley hull discussed above.

For this ship, the numerical tests have been carried and confirm that the computational domain with $\alpha = 1.0$ is large enough. The discretization of the free surface is the same as in the previous cases but the discretization of the KCS hull surface is different. The middle part of the KCS is discretized in the same way for the Wigley hull but the panels in the bow and the stern area are generated separately with their size being about 1/4 of the panels in the midship. The convert tests are also carried out with different number of panels on the free surface and on the hull surface, though not presented here for brief. The tests show that 4320 panels on half the free surface domain and 3846 panels on the half hull surface can give convergent results. The corresponding panel arrangement of KCS on the hull and free surfaces are shown in Fig. 16 and Fig. 17, respectively.

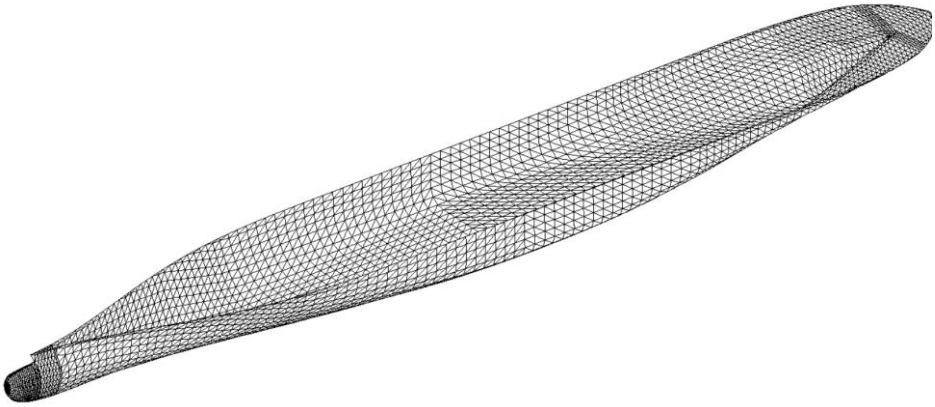

Fig. 16. Hull surface panel arrangement of KCS.

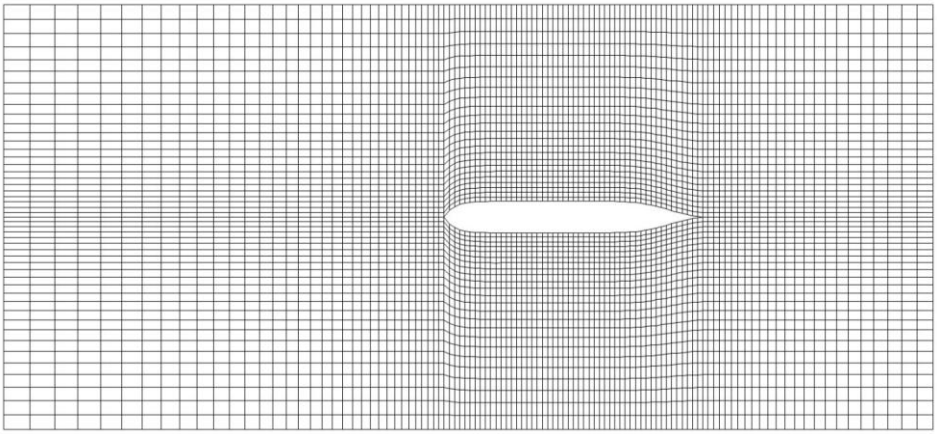

Fig. 17. Free surface panel arrangement of KCS.

The studies are carried out on the effects of the SOZ terms on the attitude of KCS using the setup in the above figures for different Froude numbers. The results are depicted in Fig. 18, together with these obtained by experiments from reference (Larsson et al., 2010) and the fully nonlinear potential simulation (Chen et al., 2016). As can be seen, the effects of the SOZ terms are generally more significant than what have been shown for the Wigley hull. More specifically, when Froude number

is larger than 0.2, the difference between computed results with and without considering SOZ can reach to 9% (e.g. in Fig.18a). Fig. 19 gives the wave profiles on the hull surface and in the longitudinal sections with $Y/L = 0.0741$ and $Y/L = 0.1509$ for the Froude number at 0.26. It shows that the wave profiles with the SOZ terms are quite different from these without the terms.

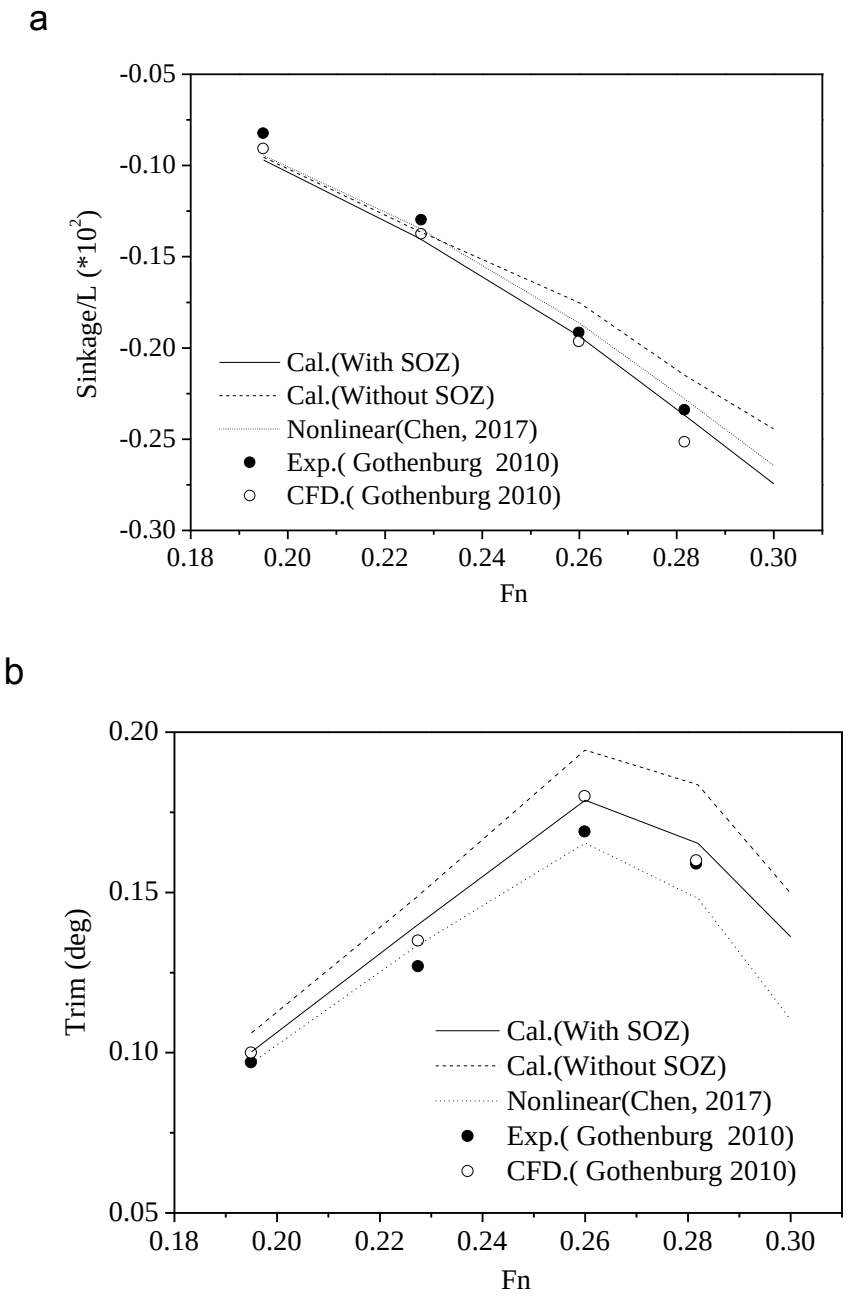

Fig. 18. Hull attitude of KCS. (a) Sinkage, (b) trim.

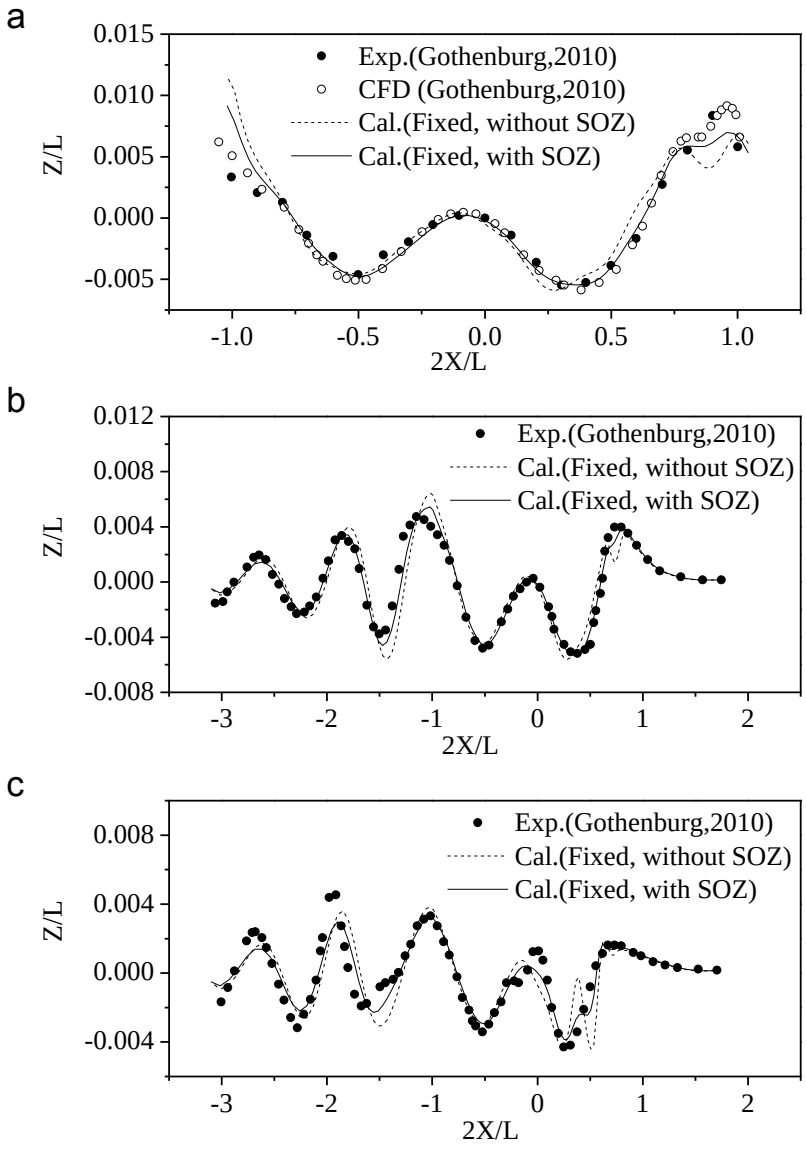

Fig. 19. Wave profiles of KCS at different sections ($F_n = 0.26$, without trim and sinkage). (a) wave profiles along ship, (b) section at $Y/L = 0.0741$, (c) section at $Y/L = 0.1509$

It is interesting to see that the computed trim and sinkage with considering the SOZ terms are much closer to experimental data than these without considering the terms. Furthermore, the results with the effects of the SOZ terms are in the similar level of accuracy as the CFD and fully nonlinear potential simulations. This seems to suggest that considering the SOZ terms can effectively account for the nonlinear effects in these cases, which are more pronounced for ships with larger block coefficients and with a higher speed.

The computed wave elevation of KCS model is shown in Fig. 20, it can be seen that with α=1, the free surface before the bow is calm and the wave reflection from the lateral boundaries is not observable in the domain. These indicate the domain used in this case is large enough and the technique used for the radiation condition is effective.

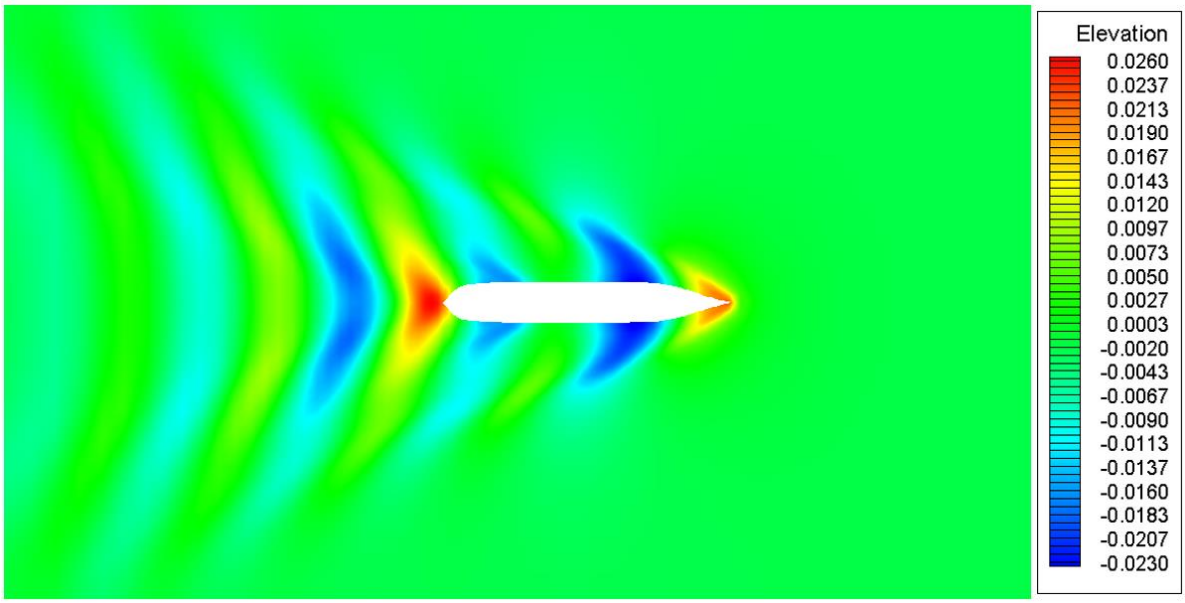

Fig. 20. Computed wave elevation of KCS model with SOZ terms at $F_n = 0.3$.

3.2 Trimarans

It is now to consider trimarans, which can advance at a high speed with the Froude number usually reaching 0.7 (Fitzsimmons V R, 2015, Bennett, 2006). Two trimarans will be considered. One is composed of three Wigley hulls (called as Tri A) and another is an actual trimaran (called Tri B).

Some experiments on the trimaran model of Tri B are carried out by the authors in the towing tank of Harbin Engineering University (HEU), which is 110m length, 7m width and 3.5m depth. The trim and sinkage of the model is measured by 4 degrees of freedom (DoFs) nautical instrument. The model has one center hull and two side hulls. The central hull and side hulls are connected by two transverse rigid links, shown in Fig. 21. Some of the results will be used for validation represented below.

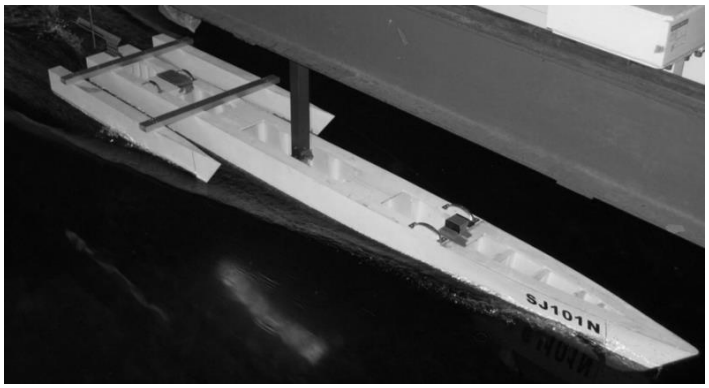

Fig. 21 Photos for experiments of Tri B in calm water

The main characteristic dimensions of its center hull of Tri B are $B/L = 0.08$, $D/L = 0.04$, $C_b = 0.52$ while these for the side hulls are $B_1/L_1 = 0.05$, $D_1/L_1 = 0.04$, $C_{b1} = 0.46$, with $x_g/L =$

-0.01, $z_g/L = 0.02$, $a/L = 0.0$, $p/L = 0.1$, where a is the longitudinal distance between the center hull stern and the side hull stern, p is the separate distance between the center hull and side hull, L_1, B_1 and D_1 are the length, the waterline breadth and the draft of side hulls, respectively, as shown in Fig. 22.

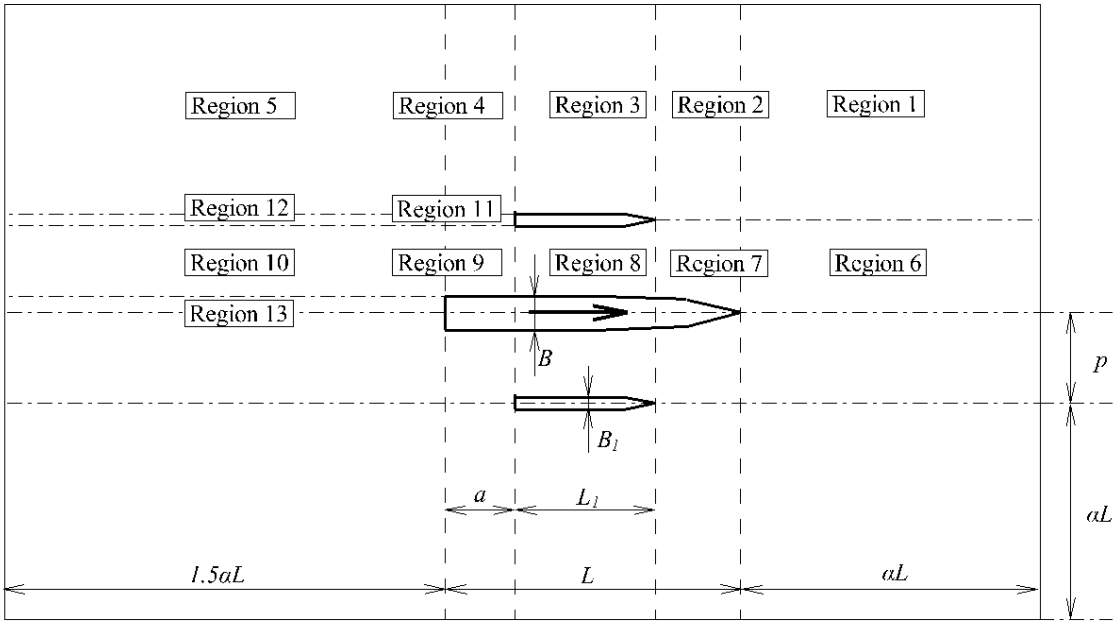

Fig. 22. Computational Domain of a trimaran

The computational domain for the trimaran cases are illustrated also in Fig. 22, which is defined in a similar way to that for monohull by the length of the domain $L_d = \alpha L + L + 1.5\alpha L$, except that the half width of the domain is $W_d = p + \alpha L$.

Similar to monohull, the hull and free surfaces of the trimaran are discretized into triangles and quadrilaterals, respectively. The meshes on the hull surfaces are generated in the same way as for the monohull described in Section 3.1, shown in Fig. 23. When discretizing the free surface, the free surface is split into sub-regions as shown in Fig. 22. The lateral lines are firstly used to split the parts of the free surface consisting of Regions 2 and 7, Regions 3 and 8, and Region 4, 11, 9, separately. The distance between two lateral lines is constant and calculated in the same way as for the free surface in the monohull cases. For the regions before the bow of the central hull and after its stern, the lateral lines are applied also in the same way as in the monohull cases. Secondly, the longitudinal lines are applied but the distance between them is different in different regions. In Regions 6-10, the number of longitudinal lines is calculated by $p/(\beta L)$, while in Regions 11-13, the number of longitudinal lines is determined by $B_t/(\beta L)$, where B_t is the width of the transom in waterplane. In Regions 1-5, the longitudinal lines are distributed again in the same way as for the area (i.e., Regions

2-3 in Fig. 7) at the side of the monohull ships. The generated mesh for the free surface is illustrated in Fig. 24.

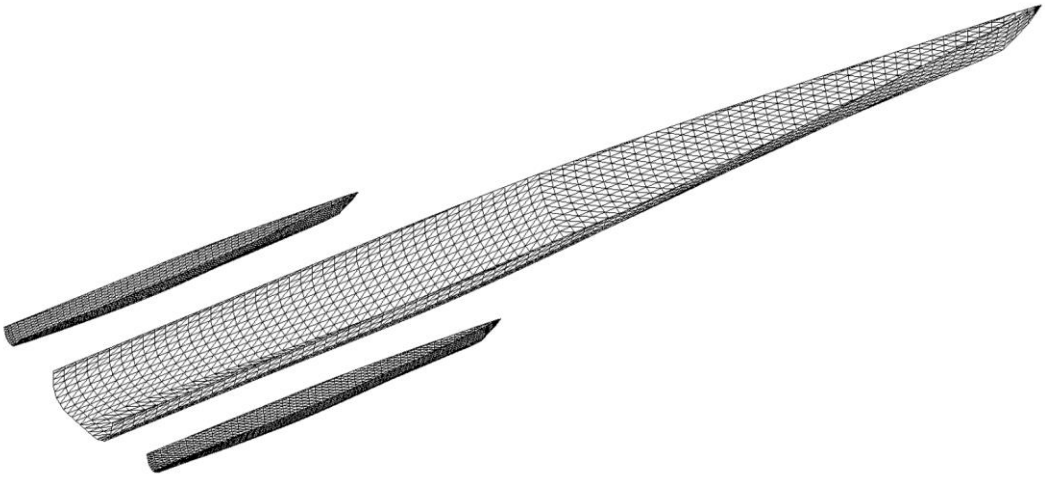

Fig. 23. Hull Surface panel arrangement for Tri B.

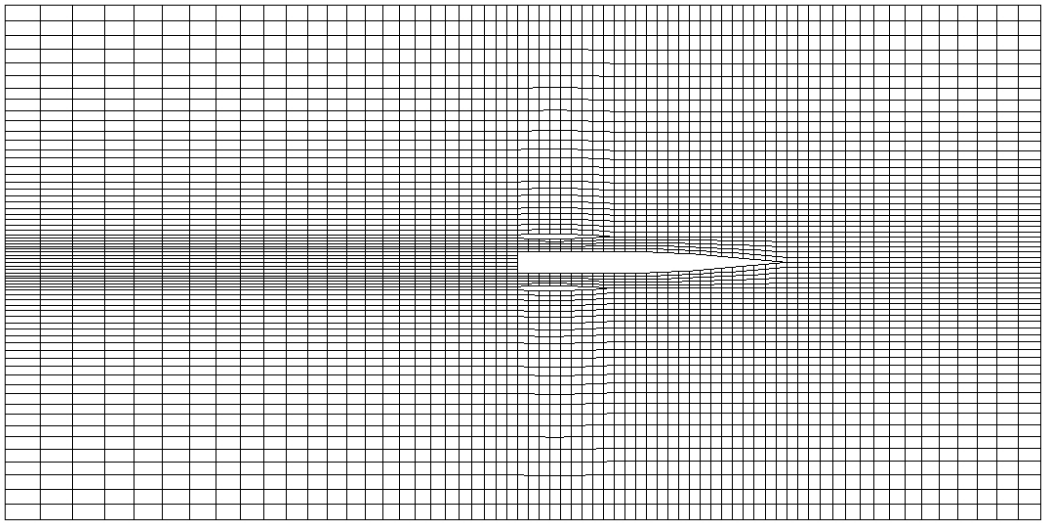

Fig. 24. Hull Surface panel arrangement of the Trimaran hull.

For the trimarans, there is no reference which gives the information about how big the computational domain should be. Therefore, the tests on the influence of domain sizes are carried out by changing the factor of α from 0.5 to 1.5. When testing the domain size, the mesh used is the same as in Case 7 in Table 4 which will be discussed later. The domain size and the corresponding computed result of Tri B at Froude number $F_n = 0.8$ are shown in Table 3. The results in the table shows that the domain size corresponding to $\alpha = 1.0$ is large enough, which will be used in other tests discussed below.

Table 3

Computed results of the attitudes of Tri B with different free surface domain sizes at $F_n = 0.8$. (with

SOZ considered).

α	L_d	W_d	with SOZ considered	
			Trim deg	Sinkage/L *10^2
0.30	$0.3L+L+0.45L$	$0.4\,L$	-0.842	-0.142
0.50	$0.5L+L+0.75L$	$0.6\,L$	-0.847	-0.145
0.70	$0.7L+L+1.05L$	$0.8\,L$	-0.836	-0.146
1.00	$1.0L+L+1.50L$	$1.1\,L$	-0.838	-0.143
1.50	$1.5L+L+2.25L$	$1.6\,L$	-0.839	-0.143

The convergent tests are also carried out for eight cases with different meshes as shown in Table 4. Table 4 also shows the computed sinkage and trim of the attitudes of Tri B for these cases. The relative errors evaluated in the same way as for Fig. 10 are presented in Fig. 25. The results show that the relative errors between Case 6-8 are less than 2%, which means that the mesh for Case 6 is fine enough. Fig. 26 shows the computed wave elevation of Tri B with SOZ terms at $F_n = 0.7$ and α=1. As already seen in Fig. 12 and Fig. 20, there is almost no wave before the bow and no wave reflection from the lateral boundaries.

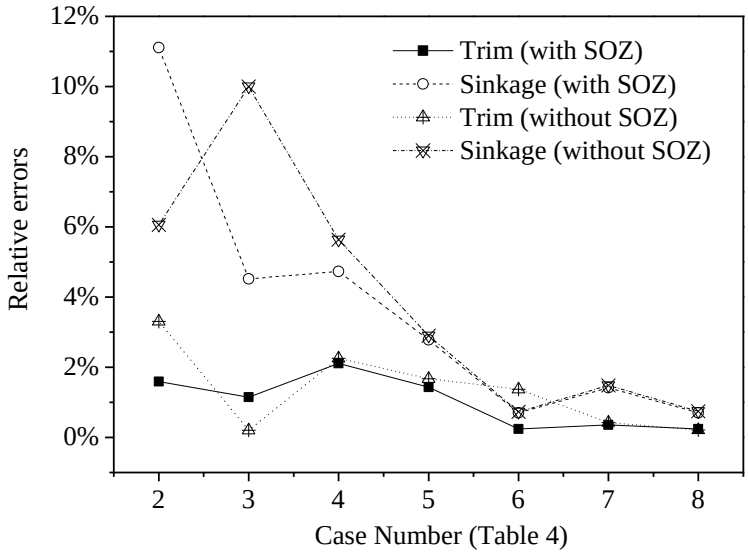

Fig. 25. Relative errors in solution with and without SOZ (Trimaran, $F_n = 0.8$).

Table 4

Computed result of the attitudes of Tri B with different number of panels at $F_n = 0.8$.

No.	Total grid number (on half domain)	Free surface (half)	Center hull (half)	One side hull (whole)	with SOZ		without SOZ	
					Trim deg	Sinkage/L *10^2	Trim deg	Sinkage/L *10^2
1	1417	1225	180	60	-0.894	-0.180	-1.031	-0.175
2	2730	2070	500	160	-0.880	-0.162	-0.998	-0.165

3	4500	2370	720	240	-0.870	-0.155	-0.996	-0.150
4	4982	2550	980	322	-0.852	-0.148	-0.974	-0.142
5	5516	2670	1280	416	-0.840	-0.144	-0.958	-0.138
6	6085	2880	1620	540	-0.838	-0.143	-0.945	-0.137
7	6620	3240	2000	660	-0.835	-0.141	-0.941	-0.135
8	8712	3960	2880	936	-0.837	-0.142	-0.943	-0.134

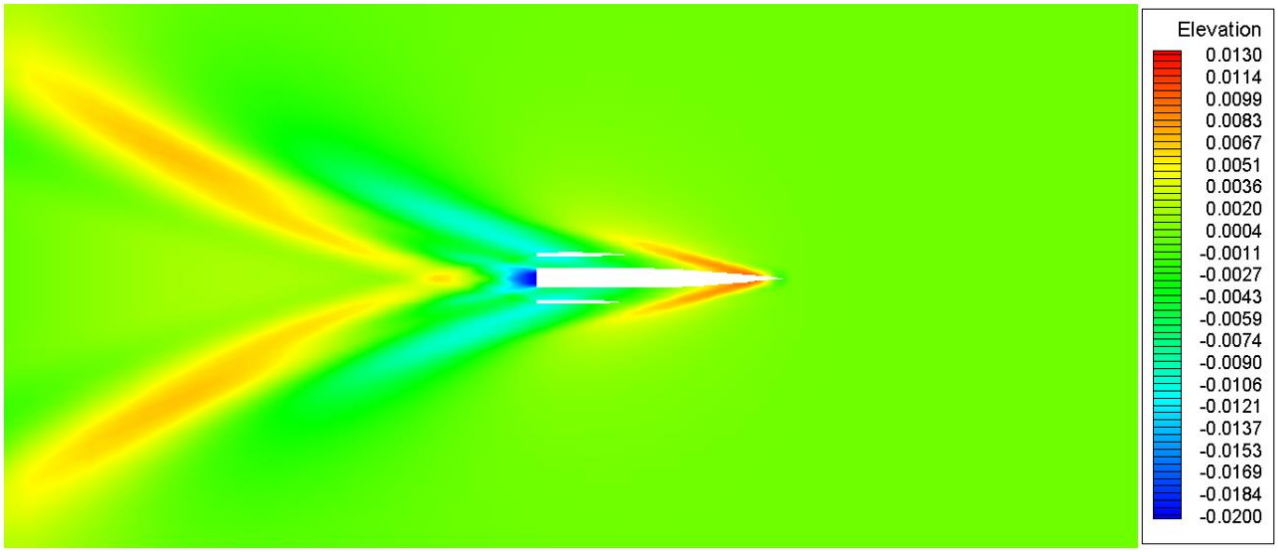

Fig. 26. Computed wave elevation of Tri B model with SOZ terms at $F_n = 0.7$.

Based on this, the effects of the SOZ terms on the attitudes of Tri B are studied for different Froude numbers using the same mesh for Case 6. Fig. 27 gives the sinkage and trim of the ship with and without considering the SOZ terms together with our experimental data. It shows that, when Froude number is larger than 0.45, the effects of the SOZ terms on the trim becomes visible, e.g., 9.8% at $F_n = 0.8$. The influence of the terms on sinkage is a bit more complex. The considerable difference between the results with and without the terms happens within the range of $F_n = 0.4$ and $F_n = 0.7$ with the maximum difference being 8.2% at about $F_n = 0.5$. In both figures, the results with considering the SOZ terms are much closer to the experimental data. It is noted that the differences caused by the terms for this ship are in the same level as for KCS, though the block coefficient here is much lower. It would be reasonable to deduce that the interaction between central and side hulls may enhance the effects of the terms.

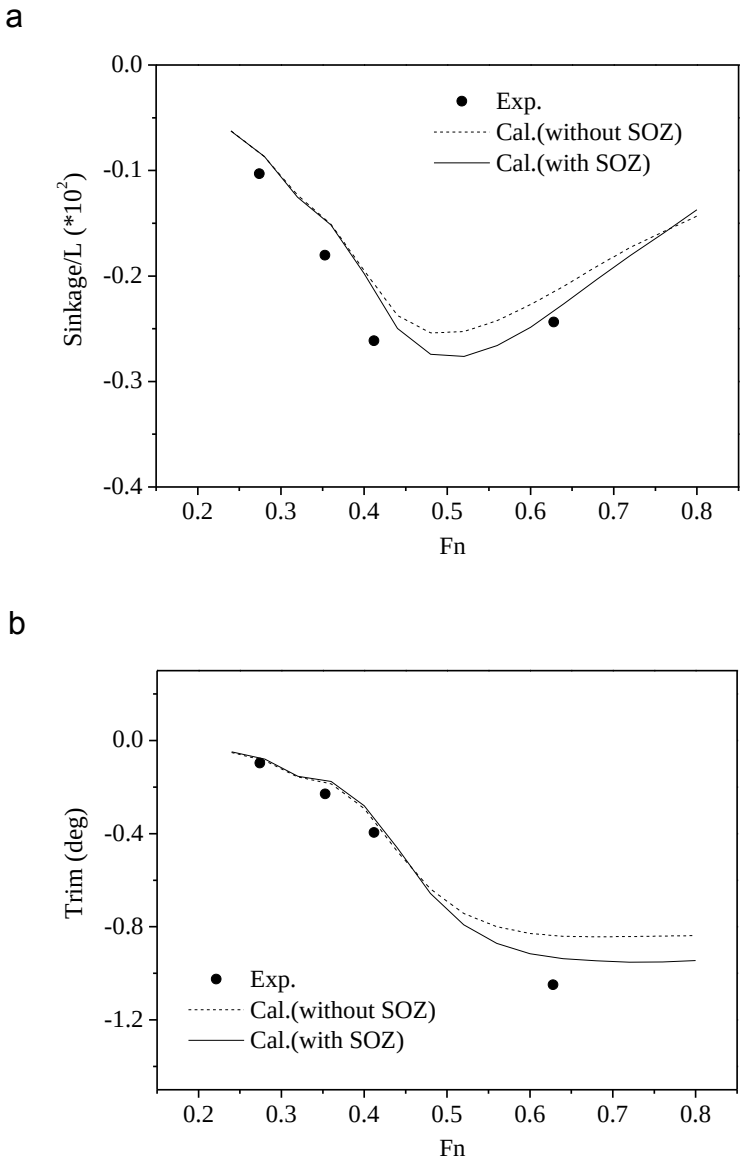

Fig. 27. Hull attitudes of the trimaran. (a) Sinkage, (b) Trim.

To further investigate whether such interaction enhance the effects, the attitudes of a trimaran composed of Wigley hulls (Fig. 28) is simulated. The main characteristic dimensions of center hull and side hulls are $C_b = 0.44,\ B/L = 0.08,\quad D/L = 0.036,\ C_{b1} = 0.44,\ B_1/L_1 = 0.44,\ D_1/L_1 = 0.36$, and the gravity center is $x_g/L = 0.0$ and $z_g/L = 0.0$. The tests on the influences of different domain sizes and meshes are also carried out for this ship and demonstrate that $\alpha = 1.0$ and the mesh similar to that in Case 6 above are appropriate. For brief, the details are not presented.

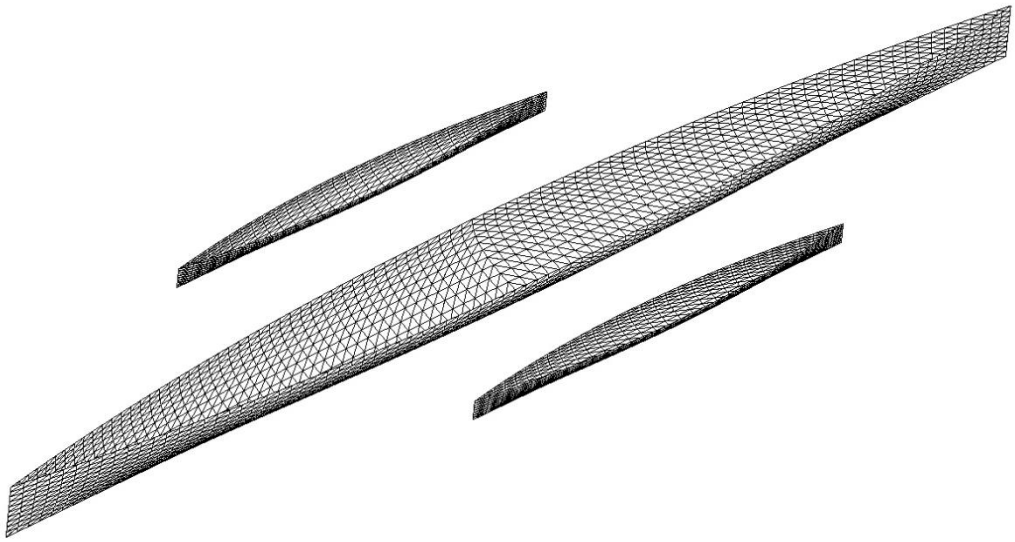

Fig. 28. Hull surface panel arrangement of the trimaran.

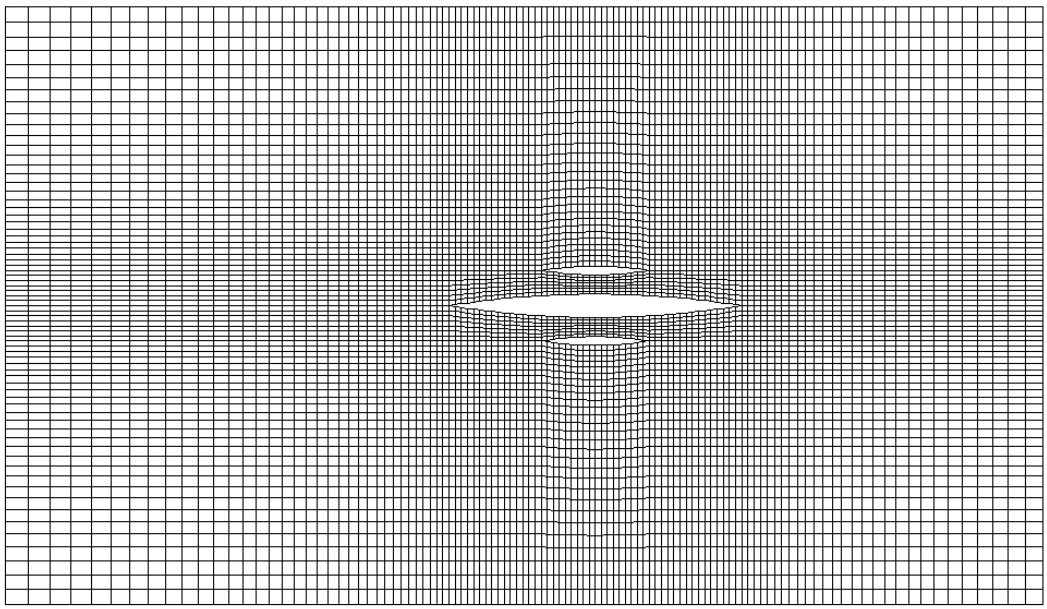

Fig. 29. Free surface panel arrangement of the trimaran.

The computed results with and without considering SOZ for the case $a/L = 0.32$, $p/L = 0.12$ and $B_1/L = 0.03$, the same as these for the model tests (Li et al., 2007), are shown in Fig. 30 together with the experimental results (Li et al., 2007). It shows that when Froude number is larger than 0.45, the sinkage with considering SOZ are very close to the experimental results while that without the terms is about 17.6% lower. The maximum difference of the trim between the cases with and without the terms occurs at about F_n=0.55, which is about 8.6%. Fig. 31 shows the coefficients of the corresponding wave-making resistance. It can be seen that the difference between the resistance coefficients with and without the SOZ terms become significant when $F_n > 0.4$ with the largest

being about 12.3% at about $F_n = 0.50$.

a

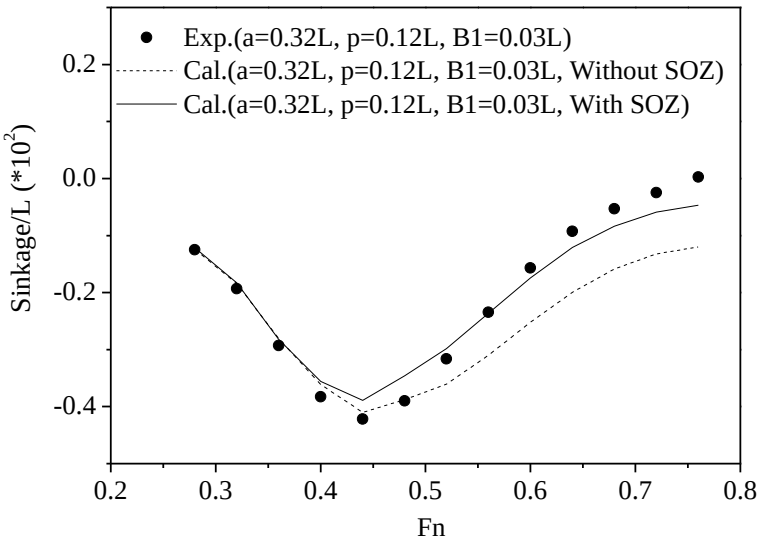

b

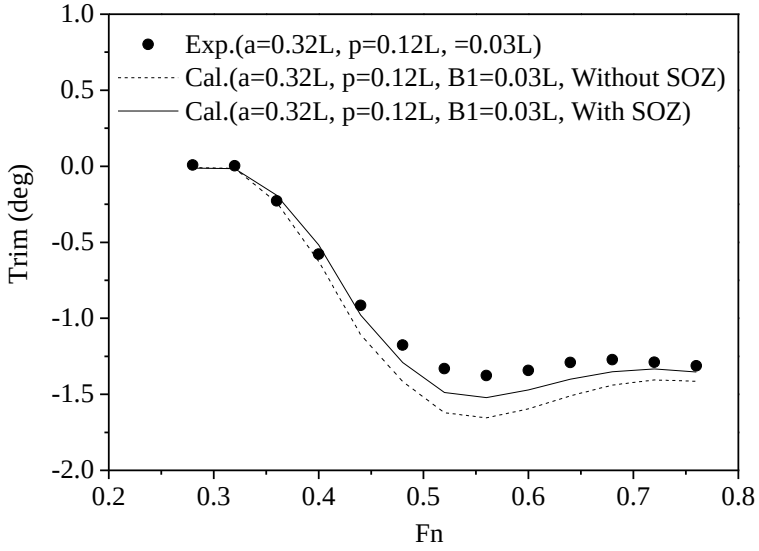

Fig. 30. Hull attitudes of the trimaran. (a) Sinkage, (b) trim.

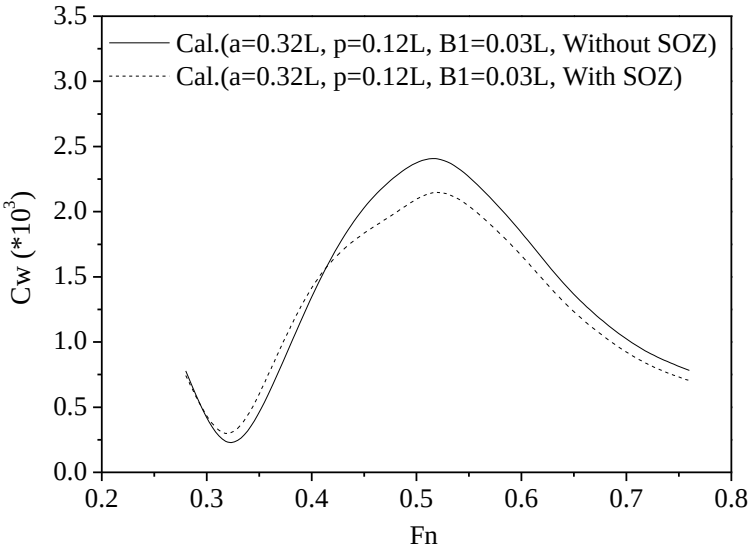

Fig. 31. Wave-making resistance of Tri A.

To shed more light on how the interaction between hulls enhances the effects of the SOZ terms, the cases with different hull separations (p) and with different side hull breadths (B_1) are investigated. For these cases, other parameters are kept the same as those for the results in Fig. 30 and Fig. 31. The relative difference between the results with and without considering the SOZ terms is estimated by the following way: $|f_1 - f_2|/f_{1,max}$, where f_1 is the computed results with the SOZ terms, f_2 is the computed result without the SOZ terms, and $f_{1,max}$ is the maximum absolute value in f_1. The relative differences are shown in Fig. 32 and Fig. 33 for sinkage, trim and wave-making resistance, respectively. One can see from Fig. 32 that when the ratio of the hull separation (p) to the ship length (L) is smaller, the effects of the SOZ terms on the sinkage become more evident, particularly at the Froude number larger than 0.5, with the maximum difference to be 30% among the cases studied. One can also see from Fig. 32 that the relative difference for the trim increase with the reduction of p/L but the largest value (~9%) occurs at about F_n=0.6. From Fig. 33 which plots the results for different side hull breadths, it is observed that the relative differences in both sinkage and trim increase with the increase of the breadths. Their maximums (about 50% for sinkage and 20% for trim) occurring at about F_n=0.6. In addition, From Fig. 32(c) and Fig. 33(c), the corresponding wave-making resistance is also significantly affected by the SOZ terms with the maximum difference being 13% in Fig. 32(c) and 28% in Fig. 33(c), respectively.

All results indicate that the hull interaction can enhance the effects of the SOZ terms. In other words, the SOZ terms may play more important role in estimating the sinkage and trim of trimaran ships than in estimating these of monohull ships.

a

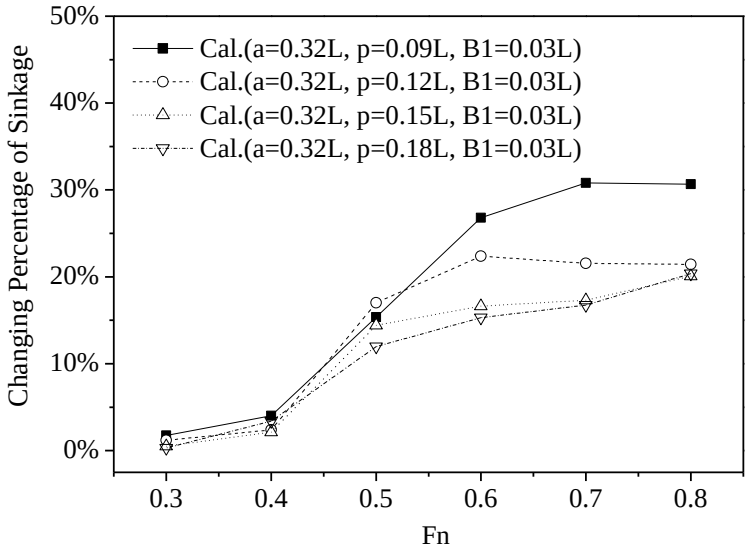
Changing Percentage of Sinkage
50%
40%
30%
20%
10%
0%
0.3
0.4
0.5
0.6
0.7
0.8
Fn
Cal.(a=0.32L, p=0.09L, B1=0.03L)
Cal.(a=0.32L, p=0.12L, B1=0.03L)
Cal.(a=0.32L, p=0.15L, B1=0.03L)
Cal.(a=0.32L, p=0.18L, B1=0.03L)

b

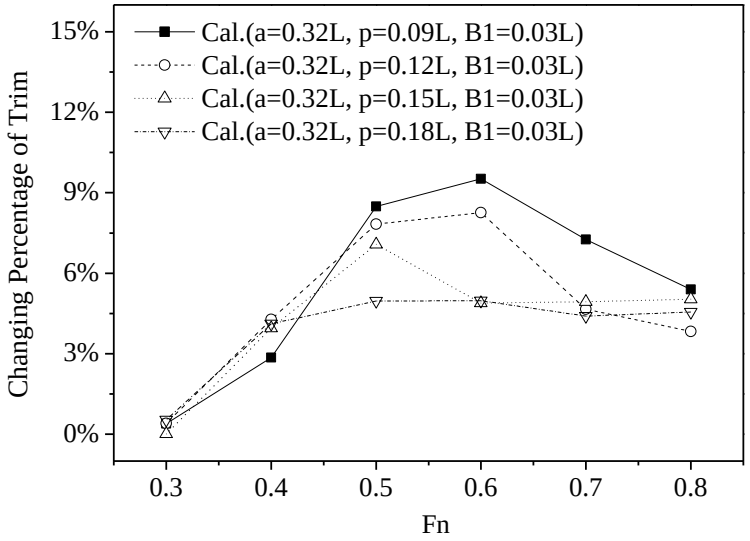
Changing Percentage of Trim
15%
12%
9%
6%
3%
0%
0.3
0.4
0.5
0.6
0.7
0.8
Fn
Cal.(a=0.32L, p=0.09L, B1=0.03L)
Cal.(a=0.32L, p=0.12L, B1=0.03L)
Cal.(a=0.32L, p=0.15L, B1=0.03L)
Cal.(a=0.32L, p=0.18L, B1=0.03L)

c

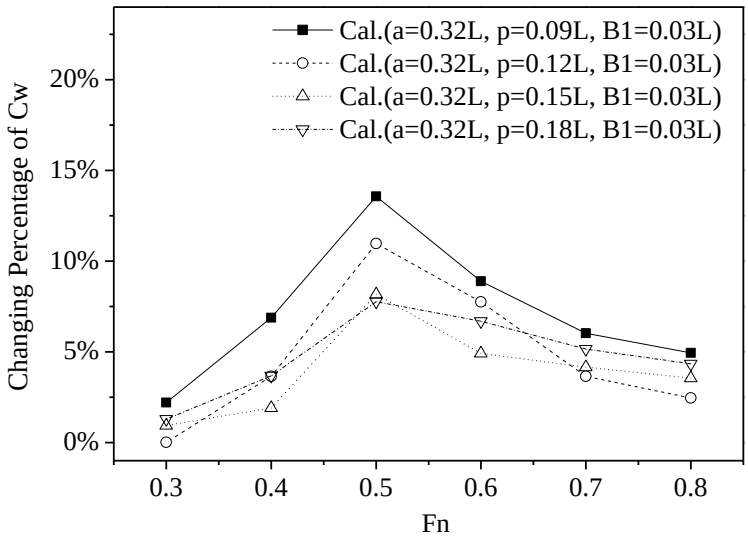

Fig. 32. Relative differences between computed results with and without considering SOZ for Tri A with different hull separations. (a) Sinkage, (b) Trim, (c) Wave making resistance.

a

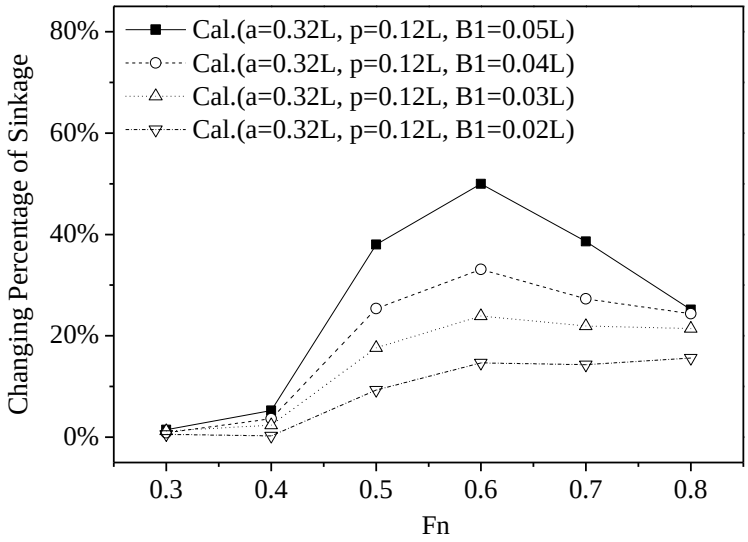

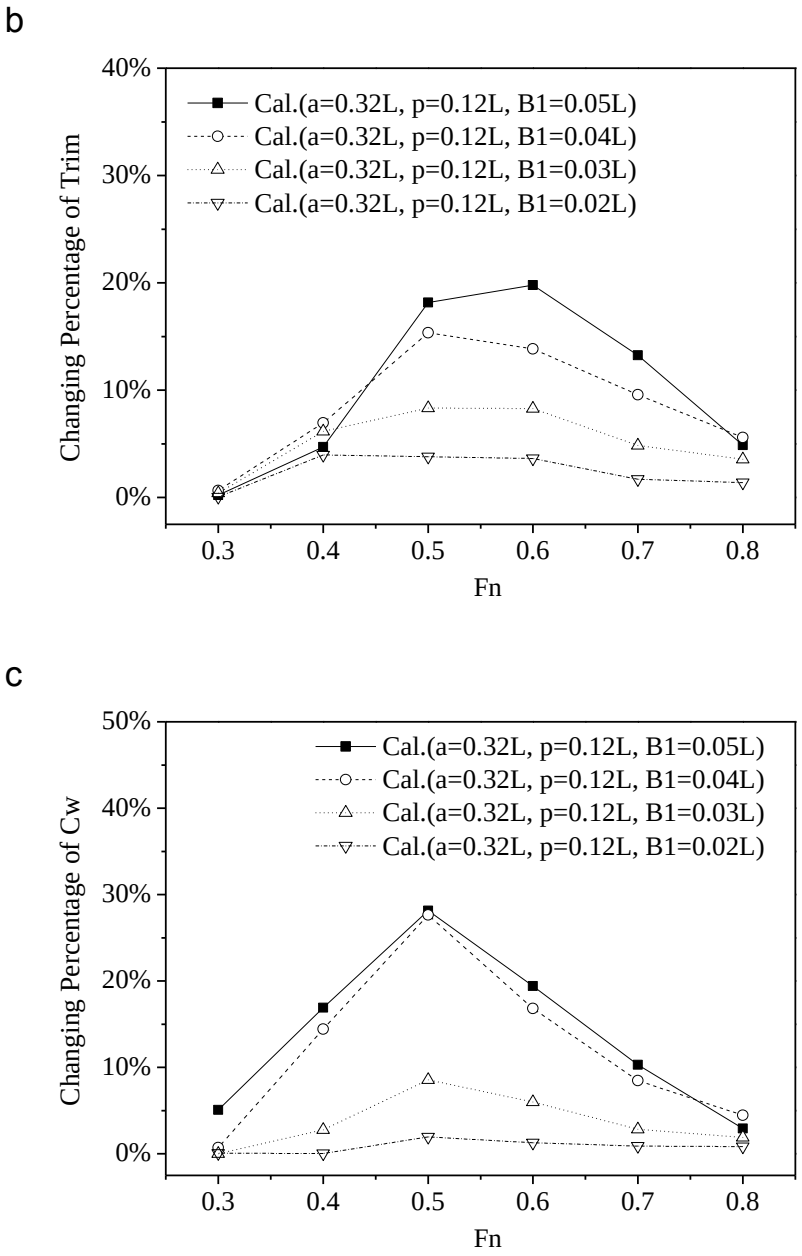

Fig. 33. Relative differences between computed results with and without considering SOZ for Tri A with different side hull breadths. (a) Sinkage, (b) Trim, (c) Wave making resistance.

3.3 Catamaran

Catamaran with two Wigley hulls is now considered. For this kind of ships, their Froude number can reach 0.75 (Davis et al., 2004). The main characteristic dimensions of each Wigley hull is the same as those for the one used in Section 4.1. The computational domain of the catamaran is shown in Fig. 34. The mesh on the hull is generated in the same way as that for Wigley hull in Section 3.1. The generation of mesh on the free surface is also similar to that case. The main difference lies in the distribution of longitudinal lines between the hulls (Regions 4-6 in Fig. 34), where the distance between the lines is constant and determined by βL. The hull and free surfaces meshes are shown in

Fig. 35 and Fig. 36. The tests similar to what have been done for the Wigley hull on different sizes of computational domain and different numbers of panels have been carried out for F_n=0.8. It is found that the domain size coefficient can be $\alpha = 1.0$, each hull surface is discretized into 3240 panels, and the panels on half the free surface is 3300.

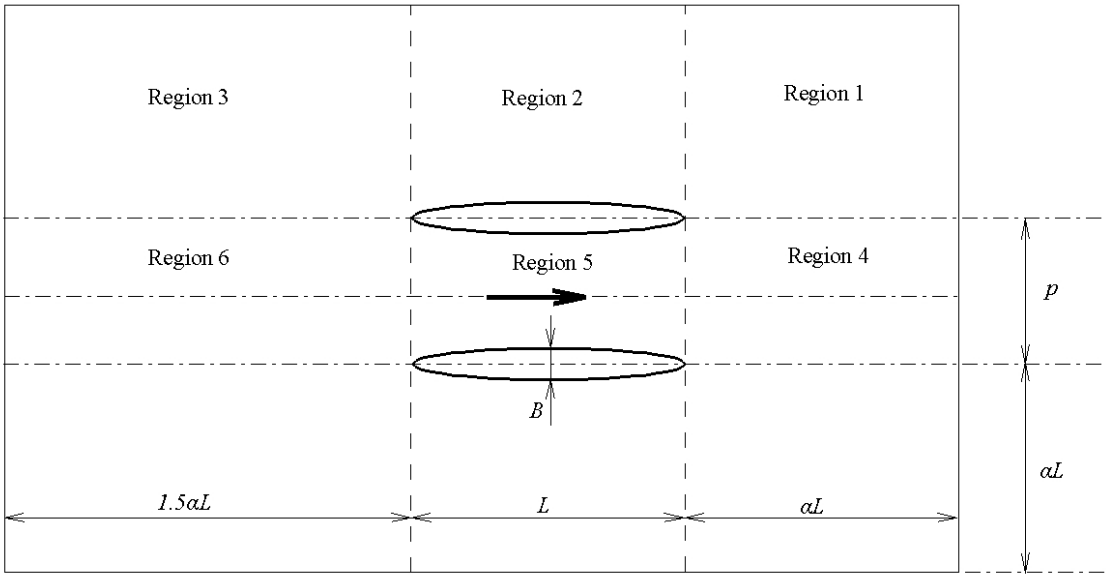

Fig. 34. Domain size of catamaran

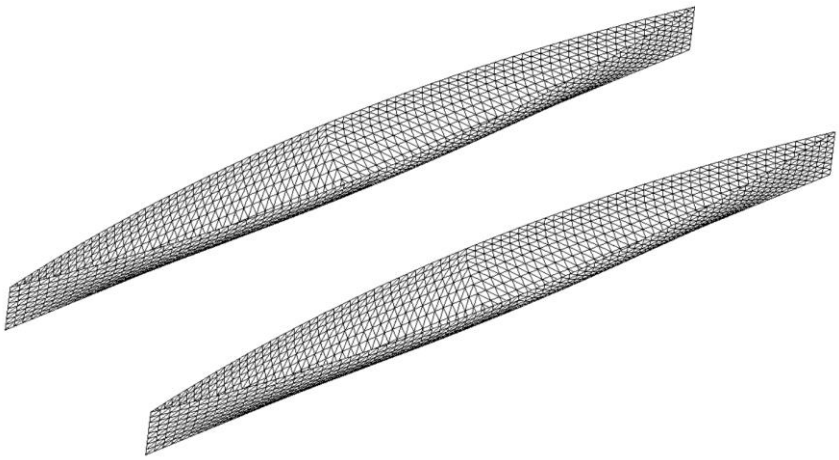

Fig. 35. Hull surface panel arrangement of the catamaran.

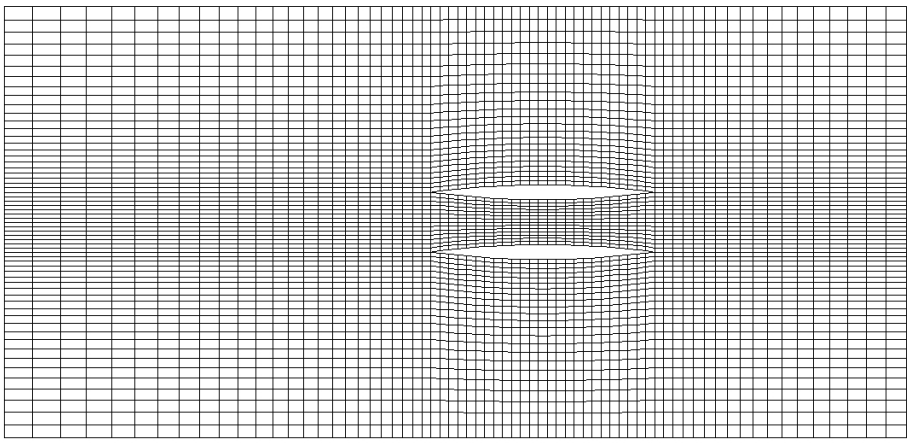

Fig. 36. Free surface panel arrangement of the catamaran.

Using the parameters, various cases are studied by varying the Froud number, the breadth of each hull and their separation. The range of separation values is chosen to be $0.2L$~$0.5L$ based on the information given by reference (Thomas et al., 2011; Souto-Iglesias et al., 2012) for real Catamarans. The relative difference (defined as the same as for Fig. 32 and Fig. 33) in the sinkage calculated by using the results with and without the SOZ terms are analyzed. The results are plotted in Fig. 37 for different separations between the hulls and in Fig. 38 for different breadths. It can be seen from these two figures that the maximum relative differences, which are considerable at some values of Froude numbers, in the sinkage, trim and resistance coefficients increase with the separation (*p/L*) being smaller and the breadth (*B/L*) being larger. Nevertheless, the magnitudes are not as large as these of the trimaran observed in Fig. 32 and Fig. 33. That is because the separation of the catamaran is bigger than the trimaran.

a

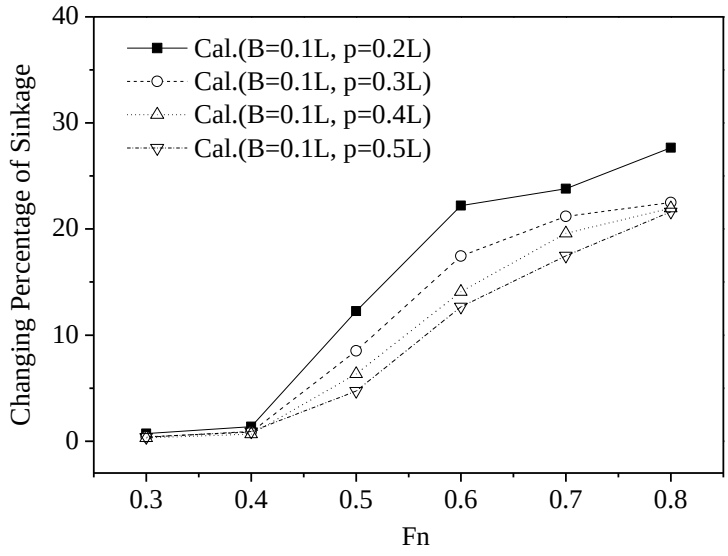

b

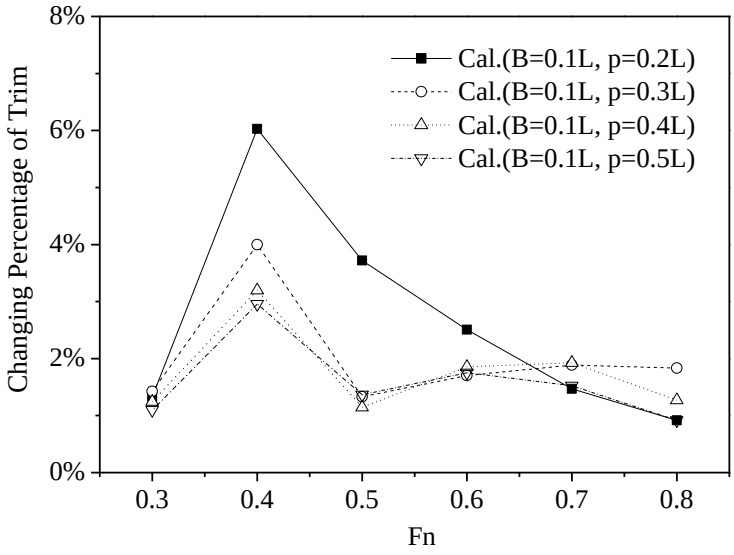

c

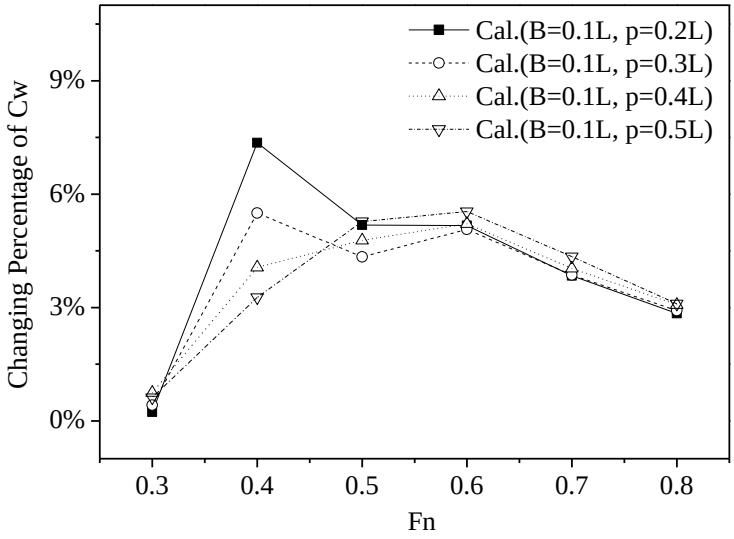

Fig. 37. Relative differences between computed results with and without considering SOZ for the catamaran with different hull separations. (a) Sinkage, (b) Trim, (c) Wave making resistance.

a

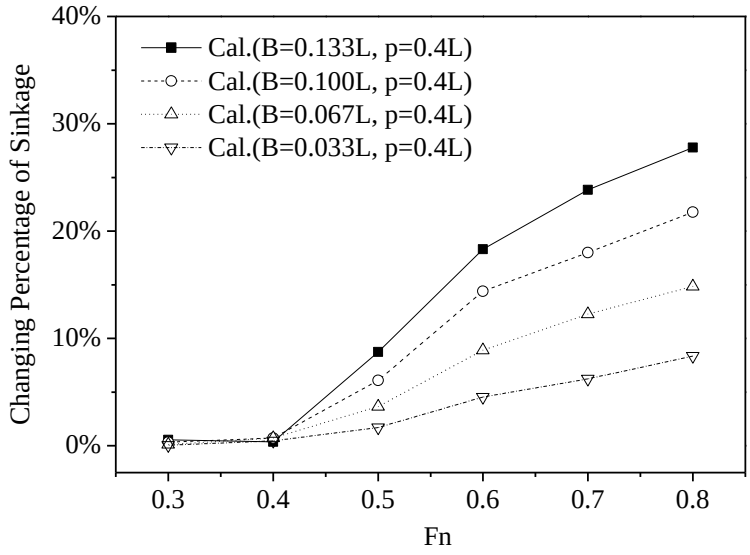
Changing Percentage of Sinkage
40%
30%
20%
10%
0%
0.3
0.4
0.5
0.6
0.7
0.8
Fn
Cal.(B=0.133L, p=0.4L)
Cal.(B=0.100L, p=0.4L)
Cal.(B=0.067L, p=0.4L)
Cal.(B=0.033L, p=0.4L)

b

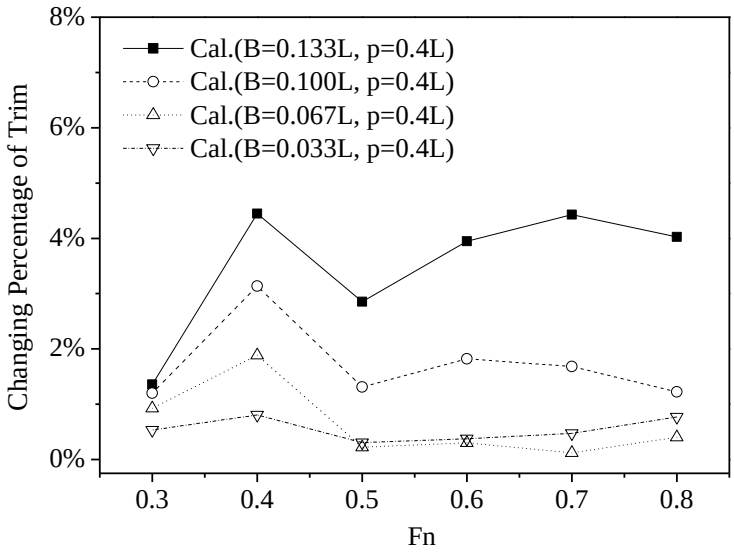
Changing Percentage of Trim
8%
6%
4%
2%
0%
0.3
0.4
0.5
0.6
0.7
0.8
Fn
Cal.(B=0.133L, p=0.4L)
Cal.(B=0.100L, p=0.4L)
Cal.(B=0.067L, p=0.4L)
Cal.(B=0.033L, p=0.4L)

c

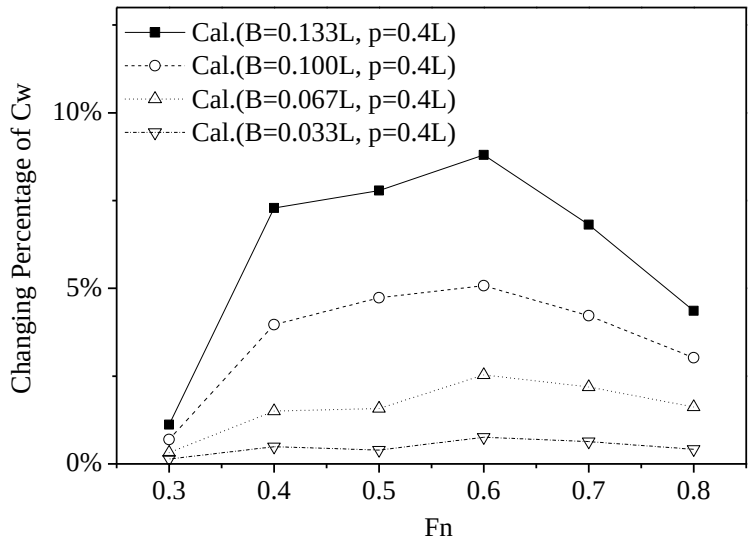

Fig. 38. Relative differences between computed results with and without considering SOZ for the catamaran with different side hull breadths. (a) Sinkage, (b) Trim, (c) Wave making resistance.

Wave patterns of different catamarans computed with and without considering the SOZ terms are compared in Fig. 39 and Fig. 40. Fig. 39 illustrates two cases for different separations and Fig. 40 depicts the cases for different breadths of the hulls. In the figures, the upper parts show the results with the SOZ terms while the lower parts give these without the terms. One can see that the discrepancy between the computed wave patterns with and without considering the SOZ terms is more apparent for the case with smaller hull separation or larger B/L, especially in the region after stern.

a

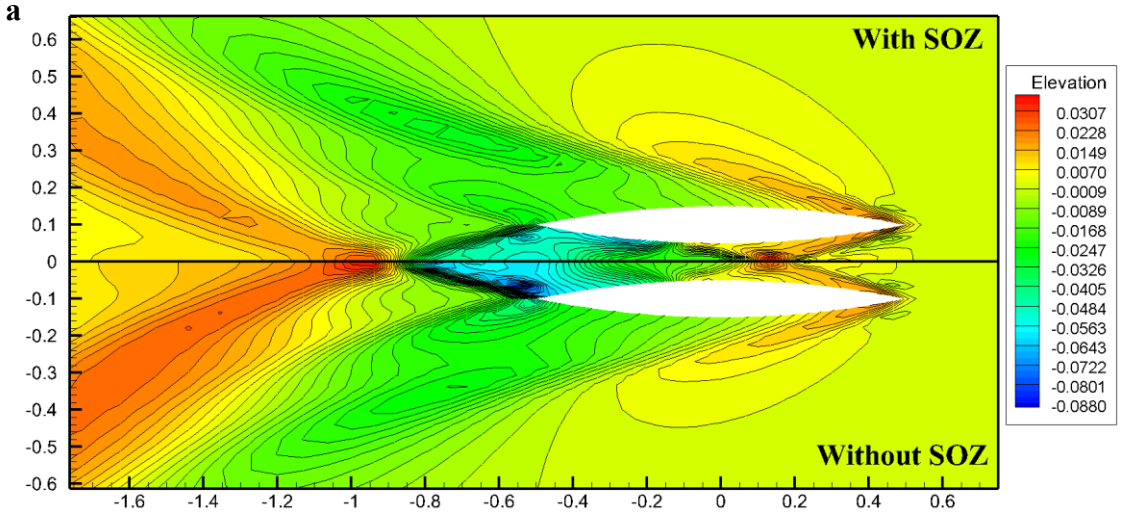

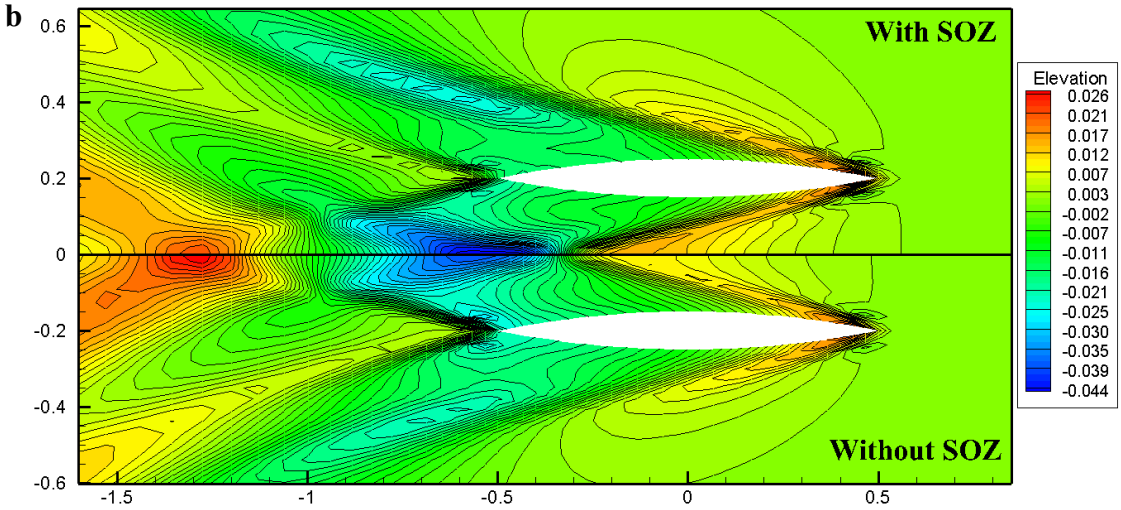

Fig. 39. Wave pattern of the catamaran with $B/L = 0.1$ at $F_n = 0.7$. (a) $p = 0.2L$, (b) $p = 0.4L$.

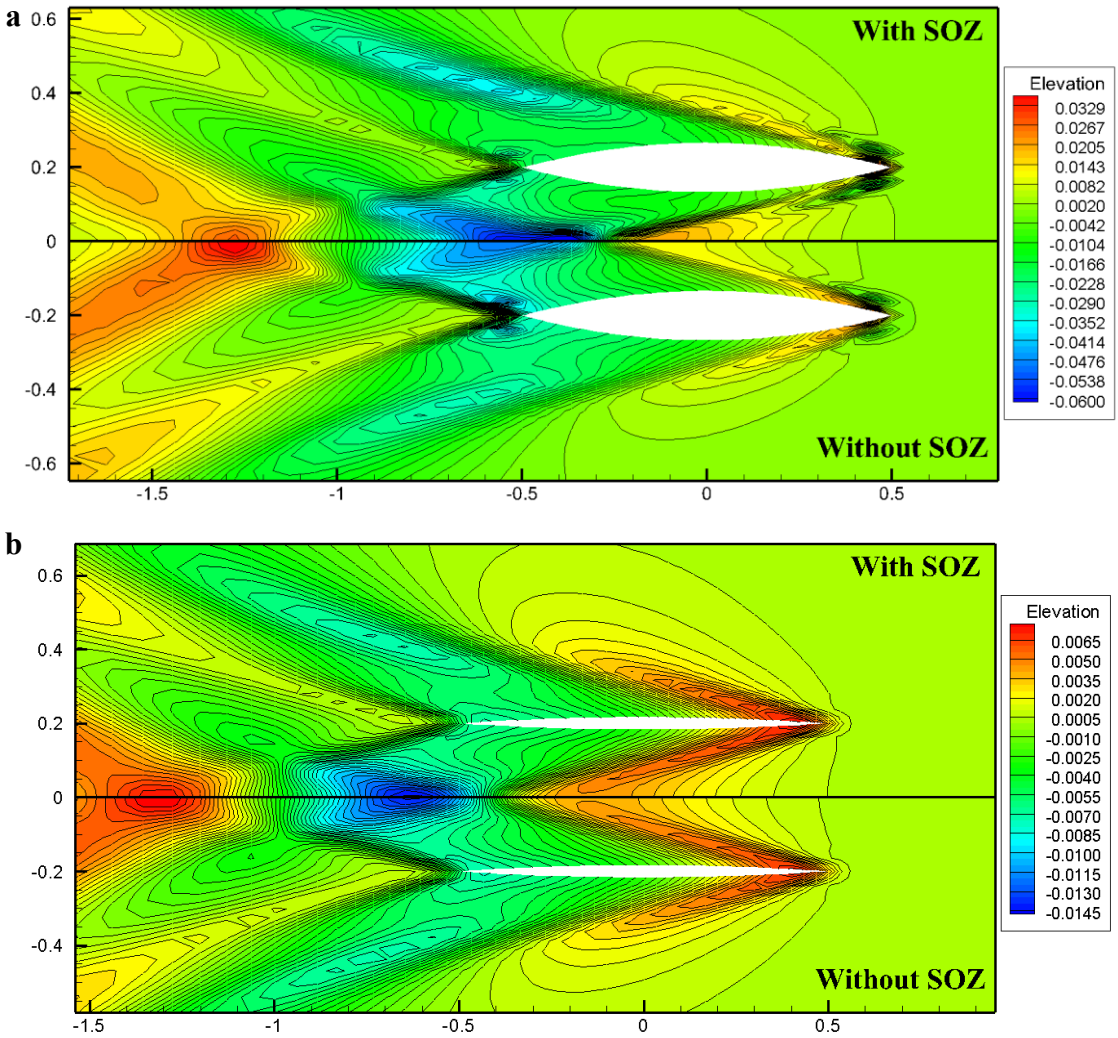

Fig. 40. Wave pattern of the catamaran with $p = 0.4L$ at $F_n = 0.7$. (a) $B/L = 0.133$, (b) $B/L = 0.067$.

5 Conclusion

In this paper, the effects of the second order derivatives in the free surface condition (i.e., the SOZ terms) on the attitudes and wave-making resistance of ships including monohull, catamaran and trimaran are studied for different parameters. For all the cases considered, careful investigations on the different numbers of panels and different sizes of computational domain are carried out. The computational results are validated by experimental data in several cases. Based on the results, the following conclusions may be drawn.

1) The SOZ terms can have visible effects on the sinkage, trim and wave-making resistance of monohull when the block coefficient and the Froude number are large; otherwise their effects can be ignored as usually done in literature.
2) For multihull ships, the effects of the SOZ terms are more pronounced. The largest difference due to the terms observed in the tested cases reaches 50%.
3) In the cases of multihull ships, the effects of the SOZ terms do not only depend on the block coeffect and Froude number but also on the interaction between the hulls. More specifically, when the interaction is stronger, such as smaller separation between hulls of trimarans and catamarans, the effects of the SOZ terms become more prominent.
4) Comparison of the results with these of fully nonlinear method shows that the results with considering the SOZ terms are in the similar level of accuracy as the CFD and fully nonlinear potential simulations. This seems to suggest that considering the SOZ terms can effectively account for the nonlinear effects in these cases for ships with larger block coefficients and with a higher speed.

According to the findings, it is recommended that the SOZ terms should be taken into account, unless there is sufficient evidence showing that their effects are negligible.

Reference

Ali, M. A., Suzuki, K., and Miyauchi, S., 2013. Study on bow wave breaking around ultra large block coefficient ship. Journal of Naval Architecture & Marine Engineering, 10(2).

Baba, E., 1979. On the free-surface conditions used by Nakatake et al. and Dawson. In: Proceedings of the Workshop on Ship Wave-resistance Computations, Vol. 2, Maryland.

Bennett, J., 2006. Creating new opportunities for high speed at sea: The Development of the Austal Auto Express 127m Trimaran. Pacific 2006 International Maritime Conference.

Chen, J. P., Zhu, D. X., and Shu-Long, H. E., 2006. Research on numerical prediction method for wavemaking resistance of catamaran/trimaran. Journal of Ship Mechanics, 10(2), 23-29.

Chen, X., Zhu, R., Ma, C., and Fan, J., 2016. Computations of linear and nonlinear ship waves by higher-order boundary element method. Ocean Engineering, 114, 142-153.

Dawson, C. W., 1977. A Practical computer method for solving ship-wave problems. II Int. Conf. Num. Ship Hydrodynamics, 30-38.

Dai, Y., 2008. Potential flow theory of ship motions in waves. National Defense Industry Publication, Beijing, 11-33.

Danışman, D.B., 2014. Reduction of demi-hull wave interference resistance in fast displacement catamarans utilizing an optimized centerbulb concept. Ocean Engineering, 91, 227-234.

Davis, M. R., Watson. N. L., and Hollowaya, D. S., 2004. Measurement and prediction of wave loads on a high-speed catamaran fitted with active stern tabs. Marine Structures, 17(7), 503-535.

Deng, R., Li, C., Huang, D., Zhou, G., 2015. The effect of trimming and sinkage on the trimaran resistance calculation. 7th International Conference on Fluid Mechanics, 126, 327-331.

Eggers, K., 1980. On the dispersion relation and exponential amplitude variation of wave components satisfying the slow ship differential equation on the undisturbed free surface, study on local non-linear effect in ship waves, Institute of Tokyo, 1980.

Fitzsimmons, V. R., 2015. Littoral Combat Ship crew scheduling. Monterey, California: Naval Postgraduate School.

IHI, SRI, U. of Tokyo and Yokohama N.U. ,1983. Cooperative Experiments on Wigley Parabolic Models in Japan.

Larsson, L., Stern, F., and Visonneau, M., 2010. A Workshop on Numerical Ship Hydrodynamics. Gothenburg, Sweden, 2010.

Li, Y., and Lu, X., 2007. An investigation on the resistance of high speed trimaran. Journal of Ship Mechanics, 11(2), 191-198.

Lv, X., Wu, X., Sun, J., and Tu, H., 2013. Trim optimization of ship by a potential-based panel method. Advances in Mechanical Engineering, 2013(7), 33-51.

Ma, C., Zhang, C., Chen, X., Jiang, Y., and Noblesse, F., 2016. Practical estimation of sinkage and trim for common generic monohull ships. Ocean Engineering, 126, 203-216.

Ma, C., Zhu, Y., Wu, H., Li, W., Huang, F., Yang, C., and Noblessea, F., 2017. Sinkage, trim, drag of a common generic freely-floating monohull ship. Applied Ocean Research, 65, 1-11.

Maruo, H., 1966. A note on the higher order theory of thin ships. Bulletin of the Faculty of Engineering 15, 1-21.

Mon, A.A., Suzukib, K., and Hino, T., 2014. Study on Bow Shape Optimization of Ultra Large Block Coefficient Ship and CFD Simulations of Initial and Optimized Hull Forms. Journal of the Japan Society of Naval Architects and Ocean Engineers, 20, 1-11.

Nakos, D. E., 1990. Ship wave patterns and motions by a three dimensional Rankine panel method. Massachusetts Institute of Technology, 1990

Peng, H., Ni, S., and Qiu, W., 2014. Wave pattern and resistance prediction for ships of full form. Ocean Engineering, 85(5), 162-173.

Raven H. C., 1989. Variations on a theme by Dawson. Symposium on Naval Hydrodynamics.

Raven, H. C., 1994. Nonlinear ship wave calculations using the rapid method. In: Sixth International Conference on Numerical Ship Hydrodynamics, Iowa City.

Raven, H. C., 1996. A solution method for the nonlinear ship wave resistance problem. Delft, Netherlands: Delft University of Technology.

Saha, K.G., and Tarafdera, M.S., 2013. Computation of Flows Around the Transom Stern Hull by the Modified Rankine Source Panel Method. Journal of Mechanical Engineering, 43(1).

Sherbaz, S., 2014. Ship Trim Optimization for Reducing Resistance by CFD Simulations. Harbin, China, Harbin Engineering University, 57-72.

Skejic, R., and Jullumstrø E., 2012. Power performance and environmental footprint of high-speed vessels in calm deep water. Proceedings of the ASME 2012, International Conference on Ocean, Offshore and Arctic Engineering, 381-393.

Souto-Iglesias, A., Fernández-Gutiérrez, D., and Pérez-Rojas, L., 2012. Experimental assessment of interference resistance for a series 60 catamaran in free and fixed trim-sinkage conditions. Ocean Engineering, 53(11), 38-47.

Suzuki, K., Kai H., and Kashiwabara S., 2005. Studies on the optimization of stern hull form based on a potential flow solver. J Mar Sci Technol, 10(2), 61-69.

Tarafdera, M. S., and Suzukib, K., 2007. Computation of wave-making resistance of a catamaran in deep water using a potential-based panel method. Ocean Engineering, 34(5), 1892-1900.

Tarafdera, M. S., and Suzukib, K., 2008a. Numerical calculation of free-surface potential flow around a ship using the modified Rankine source panel method. Ocean Engineering, 35(5), 536-544.

Tarafdera, M. S., and Suzukib, K., 2008b. Wave-making resistance of a catamaran hull in shallow water using a potential-based panel method. Journal of Ship Research, 52(1), 16-9.

Thomas, G., Winkler, S., Davis, M., Holloway, D., Matsubara, S., Lavroff, J., et al., 2011. Slam events of high-speed catamarans in irregular waves. Journal of Marine Science & Technology, 16(1), 8-21.

Wang, Z., Lu, X. and Wang, W., 2010. Fast free surface mesh generation for the calculation of trimaran wave making resistance. Journal of Harbin Engineering University, 31(4), 409-413.

Wang, Z., and Lu, X., 2011. Numerical simulation of wave resistance of trimaran by nonlinear wave making theory with sinking and trim being taken into account. Journal of Hydrodynamics, 23(2), 224-233.

Vernengo, and G., Brizzolara, S., 2017. Numerical investigation on the hydrodynamic performance

of fast SWATHs with optimum canted struts arrangements. Applied Ocean Research, 63, 76-89.

Xie, N., and Vassalos, D., 2007a. Performance analysis of 3D hydrofoil under free surface. Ocean Engineering 34(8-9), 1257-1264.

Xie, N., Vassalos, D., and Philip, S., 2007b. The effect of lift on the wave-making resistance of multi-hull craft. International Shipbuilding Progress.

Xie, N., Paton, I., and Vassalos, D., 2011. A study of hull form improvement for a fishing trawler. International Conference on Technology, Operation, Logistics and Modelling for Low Carbon Shipping.

Yasin, U., and Skir, B., 2008. Numerical Prediction of Wave Drag of 2-D and 3-D Bodies under or on a Free Surface. Turkish J. Eng. Env. Sci., 32(3), 177-188.

Zhang, B., 2009. The optimization of the hull form with the minimum wave making resistance based on Rankine source method. J. Shanghai Jiaotong Univ. (Sci.), 17(1), 65-69.

Zhang, B., 2012. Shape optimization of bow bulbs with minimum wave-making resistance based on Rankine source method, 21(2), 277-284.

Zhang, B., and Miao A., 2015a. The design of a hull form with the minimum total resistance. Journal of Marine Science and Technology, 23(5), 591-597.

Zhang, B., Miao A., and Zhang Z., 2015b. Research on design method of the full form ship with minimum thrust deduction factor, China Ocean Eng., 29(2), 301-310.